AD 740185

USCEE Report 411

DDC
RECEIVED
APR 19 1972
B

UNIVERSITY OF SOUTHERN CALIFORNIA

SEMIANNUAL TECHNICAL REPORT

Covering Research Activity During the Period
3 August 1971 through 29 February 1972

Sponsored By

Advanced Research Projects Agency

ARPA Order No. 1706

ELECTRONIC SCIENCES LABORATORY

DISTRIBUTION STATEMENT A
Approved for public release;
Distribution Unlimited

School of Engineering

Reproduced by
NATIONAL TECHNICAL
INFORMATION SERVICE
Springfield Va. 22151

Security Classification

DOCUMENT CONTROL DATA - R & D

(Security classification of title, body of abstract and indexing annotation must be entered when the overall report is classified)

1 ORIGINATING ACTIVITY (Corporate author)
Image Processing Laboratory, Electronic Sciences Laboratory, University of Southern California, University Park, Los Angeles, California 90007

2a. REPORT SECURITY CLASSIFICATION
UNCLASSIFIED

2b. GROUP

3 REPORT TITLE
Semiannual Technical Report to the Director, Advanced Research Projects Agency, for the period 3 August 1971 to 29 February 1972

4 DESCRIPTIVE NOTES (Type of report and inclusive dates)
Technical Semiannual 3 August 1971 to 29 February 1972

5 AUTHOR(S) (First name, middle initial, last name)
William K. Pratt (project director)

6 REPORT DATE

7a. TOTAL NO. OF PAGES
53

7b. NO. OF REFS
26

8a. CONTRACT OR GRANT NO
F08606-72-C-0008

b. PROJECT NO
ARPA Order No. 1706

c.

d.

9a. ORIGINATOR'S REPORT NUMBER(S)
USCEE Report 411

9b. OTHER REPORT NO(S) (Any other numbers that may be assigned this report)
None

10 DISTRIBUTION STATEMENT
Approved for public release; distribution unlimited

11 SUPPLEMENTARY NOTES

12. SPONSORING MILITARY ACTIVITY
Advanced Research Projects Agency
1400 Wilson Blvd.
Arlington, Virginia 22209

13 ABSTRACT

This technical report summarizes the image processing research activities performed by the University of Southern California during the period of 3 August 1971 to 29 February 1972 under Contract No. F08606-72-C-0008 with the Advanced Research Projects Agency, Information Processing Techniques Office. The research program, entitled, "Image Processing Research," has as its primary purpose the anlysis and development of techniques and systems for efficiently generating processing, transmitting, and displaying visual images and two dimensional data arrays. Research is oriented toward digital processing and transmission systems. Four task areas are reported on: (1) Image Analysis Projects, the development of quantitative measures of image quality; (2) Image Coding Projects, the investigation of digital bandwidth reduction coding methods; (3) Image Enhancement and Restoration Projects, the improvement of image fidelity and presentation format; (4) Image Processing Support Projects, a description of the U.S.C. Image Processing facilities and support projects.

DD FORM 1 NOV 68 1473

UNCLASSIFIED
Security Classification

Security Classification

14 KEY WORDS	LINK A		LINK B		LINK C	
	ROLE	WT	ROLE	WT	ROLE	WT
Image Processing						
Digital Image Processing						
Image Coding						
Image Enhancement						
Image Restoration						
Image Processing Languages						
Color Image Processing						
Digital Image Transforms						
Pseudocolor Processing						
Image Processing Bibliography						

Security Classification

USCEE Report 411

SEMIANNUAL TECHNICAL REPORT

Covering Research Activity During the Period
3 August 1971 through 29 February 1972

William K. Pratt
Project Director
(213) 746-2694

Image Processing Laboratory
Electronic Sciences Laboratory
University of Southern California
University Park
Los Angeles, California 90007

Details of illustrations in
this document may be better
studied on microfiche

This research was supported by the Advanced Research Projects Agency of the Department of Defense and was monitored by the Air Force Eastern Test Range under Contract No. F08606-72-C-0008, ARPA Order No. 1706

The views and conclusions in this document are those of the authors and should not be interpreted as necessarily representing the official policies, either expressed or implied, of the Advanced Research Projects Agency or the U. S. Government.

ABSTRACT

This technical report summarizes the image processing research activities performed by the University of Southern California during the period of 3 August 1971 to 29 February 1972 under Contract No. F08606-72-C-0008 with the Advanced Research Projects Agency, Information Processing Techniques Office.

The research program, entitled, "Image Processing Research," has as its primary purpose the analysis and development of techniques and systems for efficiently generating, processing, transmitting, and displaying visual images and two dimensional data arrays. Research is oriented toward digital processing and transmission systems. Four task areas are reported on: (1) Image Analysis Projects, the development of quantitative measures of image quality; (2) Image Coding Projects, the investigation of digital bandwidth reduction coding methods; (3) Image Enhancement and Restoration Projects: the improvement of image fidelity and presentation format; (4) Image Processing Support Projects, a description of the USC image processing facilities and support projects.

PROJECTS PARTICIPANTS

Project Director

William K. Pratt

Research Faculty

Harry C. Andrews
Lee D. Davisson
Ali Habibi
Anil K. Jain
Richard P. Kruger
Nasser Nahi
Alexander A. Sawchuk
Lloyd R. Welch

Support Staff

Angus B. Cossey
Carolyn Matthews
Robert E. Mikhel
Mark A. Sanders
Michael Reichik
Linda M. Webster

Students

Tooraj Assefi
Wen-Hsiung Chen
Roy M. Glantz
Kripa Goswamy
Richard Keegan
David Levy
Clanton Mancill
Scott Minium
Manuher Naraghi
Sumeet Pasricha
James Pepin
Clifford Reader
Stuart Robinson
Edward Sutton
Carl Wedberg

TABLE OF CONTENTS

LIST OF FIGURES

LIST OF FIGURES (cont'd)

1. Introduction

This report describes the progress and results of the University of Southern California image processing research study for the period of 3 August 1971 to 29 February 1972.

The image processing research study has been subdivided into five projects:

Image analysis projects
Image coding projects
Image restoration/enhancement projects
Image detection projects
Image support projects

The image analysis project comprises the background research effort into the basic structure of images in order to develop meaningful quantitative characterizations of an image. In image coding the orientation of the research is toward the development of digital image coding systems that represent monochrome and color images with a minimal number of code bits. Image restoration is the task of improving the fidelity of an image in the sense of compensating for image degradations. In image enhancement, picture manipulation processes are performed to provide a more subjectively pleasing image or to convert the image to a form more amenable to human or machine analysis. The objective of the image detection projects is the recognition, classification, and identification of objects within pictures. Finally, the image research projects include research on image processing computer languages and the development of experimental equipment for the sensing, processing, and display of images.

The following sections describe the research effort on the image processing projects listed above, with the exception of the image detection projects. Reporting of results on the image detection projects is being deferred to the next reporting period.

2. Image Analysis Projects

In the development of image coding, enhancement, and detection processes it is convenient, and often necessary, to quantitatively characterize the image to be processed. A continuing study is underway to determine and assess quantitative image measures. One class of measures under consideration is the "high fidelity" measure of small differences in image quality. Another class of measures are those associated with the intelligibility of a degraded image.

One part of the general problem of specifying an image measure that has been studied during the past six months is the development of a color difference measure between two colors defined by trichromatic color coordinates. The color difference measure has found application in the design of quantization and coding systems for digital color representation.

2.1 Digital Color Measure

Anil K. Jain

Quantitative measures of color difference for any two arbitrary colors in a suitable color coordinate system based on tristimulus or luminance/chromaticity values is a problem of considerable interest in coding, enhancement, recognition and detection of color images. Experimental evidence has led to the belief that the tristimulus color solid may be considered as a Riemmanian space and that the color distance metric may be described by

$$(ds)^2 = \sum_{i=1}^{3} \sum_{j=1}^{3} c_{ij}\, dx_i\, dx_j$$

where dx_i, $i = 1,2,3$ represents the infinitesimal difference between two colors with coordinates x_i and $x_i + dx_i$ in the chosen color coordinate system. The coefficients c_{ij} measure the average human perception

sensitivity of small differences in the i^{th} and in j^{th} coordinates.

The study of small differences in color described above is based on observations of "just noticeable differences" (JND) in colors. A unit JND defined by

$$1 = \sum_{i=1}^{3} \sum_{j=1}^{3} c_{ij} dx_i dx_j$$

is the describing equation for an ellipsoid. The distance between any two arbitrary colors c_1 and c_2 is then given by the minimal distance chain of the ellipsoids as specified by

$$d = \min_{x_i} \int_{c_1(x_1)}^{c_2(x_i)} ds$$

Solution of this equation requires the determination of a geodesic in a three dimensional Riemmanian color space. It has been found that evaluation of the geodesic by the calculus of variations results in a nonlinear boundary value problem of considerable complexity, and that the dynamic programming solution encounters dimensionality restrictions [1]. A computer program to determine the geodesic iteratively by a gradient technique has proven successful [2]. In the program convergence is obtained quite rapidly (6 to 7 iterations). Figure 2.1-1 contains a plot of the geodesic curves between several colors on the Uniform Chromaticity Scale chromaticity diagram. The distance along each curve is the metric distance measure between each color. The geodesics between the primaries are nearly straight lines, but the geodesics between most other colors are generally curved. These analytic results are presently being evaluated by subjective experimentation.

References

1. A. K. Jain, "Color Distance and Geodesics in Color-3 Space," USCEE Technical Report No. 411, March 1972, Image Processing Laboratory, University of Southern California, Los Angeles, California.

2. E. J. Muth and C. G. Persels, "Computation of Geodesics in Color-3 Space by Dynamic Programming," Proceedings of the Fourth Hawaii Conference on System Sciences, January 1971, pp. 155-157.

3. A. K. Jain and W. K. Pratt, "PCM Coding of Color Images Via Color Distance," (in preparation).

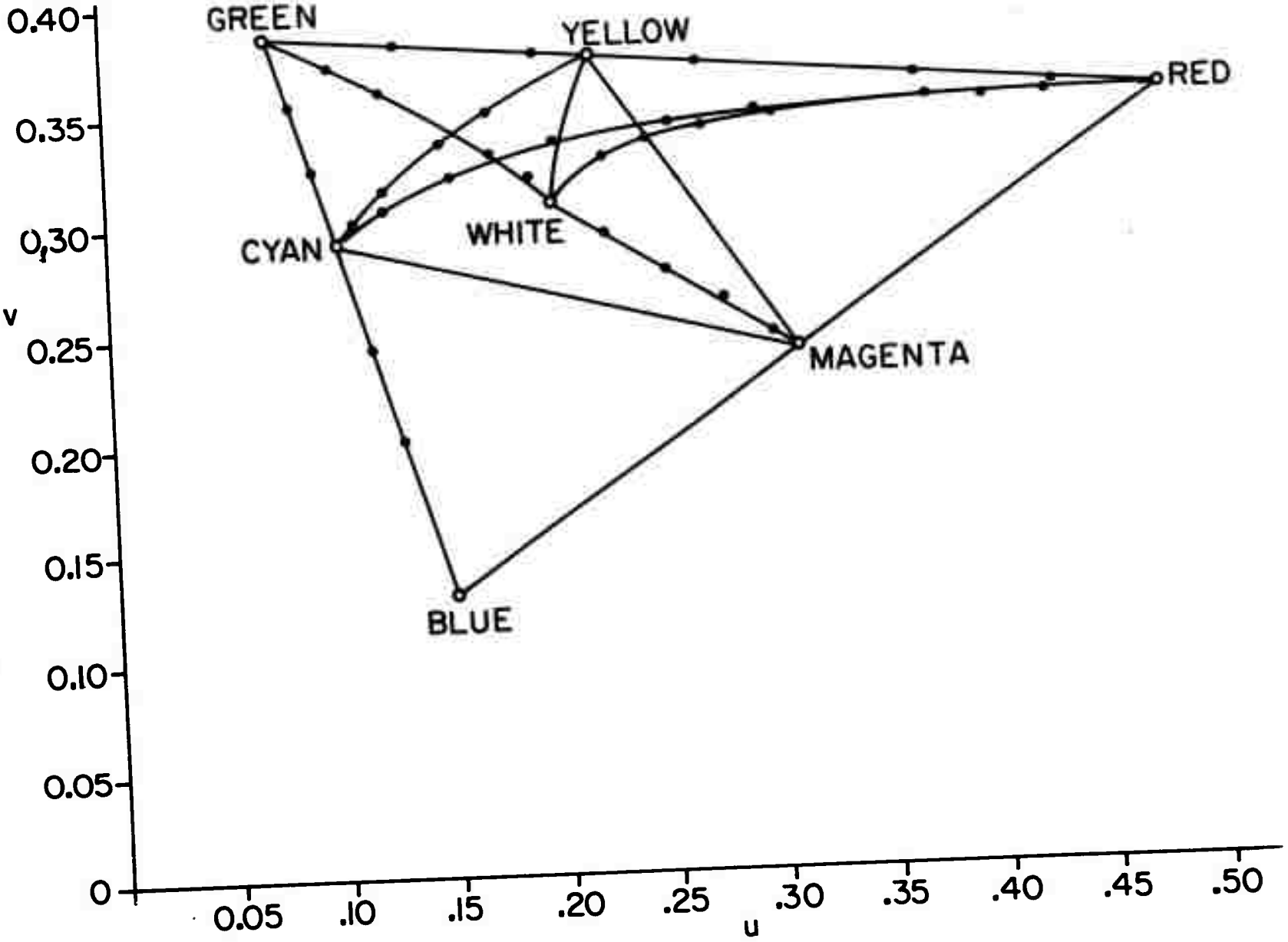

Figure 2.1-1 Example of geodesic color distances

3. Image Coding Projects

Perhaps the greatest immediate need from image processing research is the invention of efficient image coding systems. Ultimately, research will probably result in the development of a family of image coding systems geared to specific applications, the amount of implementation complexity permitted in the design, and the permissible image degradation, rather than an all-purpose single design image coder.

During the past six months the image coding research effort has been concentrated in three major areas: the design of information preserving image coders; the study of differential PCM coders for color imagery; and improvements and extensions of the transform coding systems for monochrome and color images. The information preserving coder is capable of reducing the channel rates for monochrome images to about 3 bits/pixel for an original of 6 bits/pixel, and can operate at rates comparable to the ARPA net transmission rate. The differential PCM coder results in coding with about 2 to 3 bits/pixel for monochrome images and 6 to 8 bits/pixel for color images with a small amount of distortion and a reasonably simple implementation. The transform coders under investigation approach rates of 1 bit/pixel for monochrome pictures and 2.0 bits/pixel for color images with a little distortion. Implementation of the transform coders is somewhat more complex than for a differential PCM coder, but is feasible for up to real time TV rates.

3.1 Information Preserving Image Coding*

Lee D. Davisson

In recent years the ability has been created to generate large quantities of earth-observational data and to apply sophisticated processing to that data for many purposes. Principal among these are meteorological observations for the many aspects of weather prediction. The use of

*This work is partially supported under NASA Contract NAS 5-21505.

satellites to acquire images of the earth on an operational basis has dramatically increased the amount of data involved in weather prediction. These data are transmitted from various stations to a central location for computer processing. The data rate requirements and hence the transmission costs are high, providing ideal applications for data compression. At the same time data quality must be maintained at a high level for use in machine processing.

One of the data sources under study is the Applications Technology Satellite (ATS). The ATS image line rate is determined by the spin period of the spacecraft, nominally 600 milliseconds. The data processed is from the ATS spin scan camera which sweeps one image line per revolution. A full earth image takes about 20 minutes. Since the ATS spacecraft are in synchronous orbit, the earth subtends an angle of 18 degrees or 1/20 of a revolution. The video data is obtained from a photomultiplier tube in the spin scan camera which observe the earth for only 30 msec. per scan line. The data is transmitted in analog form to the receiving station where it is digitized for transmission to the central processing location. A special synchronizing circuit provides a pulse to indicate when the A/D converter should begin to operate for the 30 msec. of useful data for each 600 msec. period. The sampling rate and digital resolution depends upon the user requirements and the transmission capability. Nominal characteristics are 4096 samples per line with 6 bits of resolution.

The goal set for the data compression system study is to attain a minimum reduction in transmission rate (compression ratio) of two to one with six bits per sample resolution and no error or eight bits per sample resolution with a maximum of one quantization level error. The data compression algorithm must at the same time be capable of performing in real time at the rates described above.

Statistical studies on digital tape data have found the following

algorithm to be capable of meeting the data compression goals. The algorithm forms the successive sample-to-sample differences and encodes the differences up to some maximum magnitude using a variable length code. When the difference exceeds the maximum magnitude, the sample value itself is sent with an appropriate prefix to distinguish this from a difference code word. The code words are chosen by using the Shannon-Fano encoding procedure with empirical frequencies for the relative probabilities. In particular, zero difference is encoded by a single "one" bit.

The above procedure was found to result in a code whose efficiency is greater than 90%. The codes are characterized by leading zeros, the exact number of which determines each code word's length. This procedure can be used to simplify the decoding.

When redundancy is removed, the data quality becomes more sensitive to channel errors. To combat this effect controlled redundancy is added in the form of synchronization words. In addition to the usual line synch, data synch words are periodically inserted in the encoded data after each fixed number of encoded samples. Following synchronization the actual sample value is sent rather than the sample difference to eliminate any built up error.

Since variable length encoding is used for transmission over a fixed rate channel, a buffer must be provided to hold the encoded data prior to transmission. To prevent buffer underflow, a transmission delay of several lines is provided to allow the buffer to partially fill. The exact required buffer length and transmission delay are currently under study.

Figure 3.1-1 is an ATS picture which has been compressed at a compression ratio of approximately 2 to 1 and reconstructed using the preceding technique. The synchronization errors result from a deficiency of the experimental transmission system, and are not a consequence of the coding system.

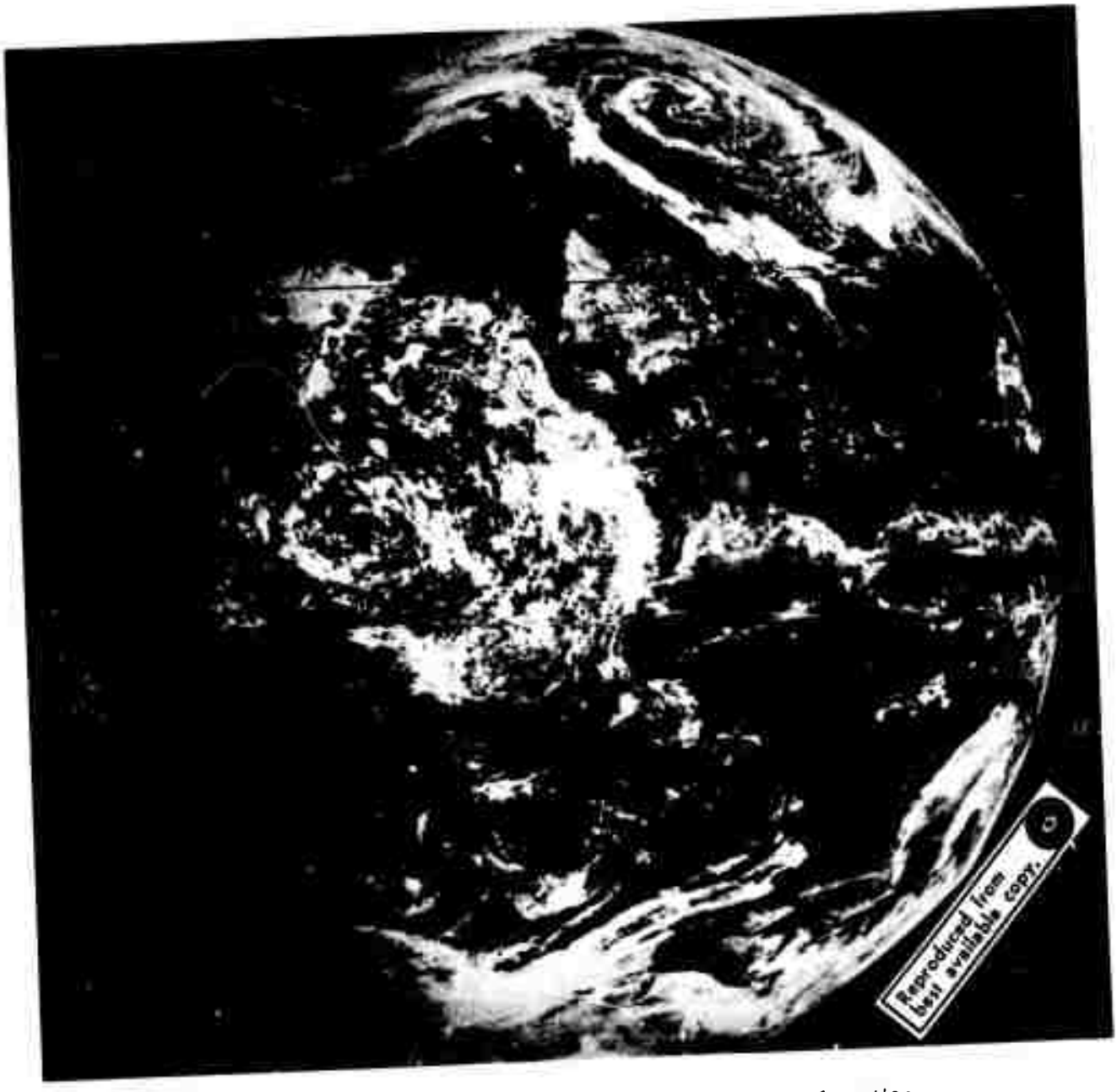

Figure 3.1-1. Compressed ATS colored picture using information preserving coding of pixel differences - 3.0 bits/pixel.

3.2 Differential PCM Coding of Color Images

A. Habibi

In a differential PCM system a differential signal is formed between the information source and a predicted signal based upon the past states of the source. Differential PCM is potentially more efficient than standard PCM because: 1) the differential signal is less correlated, and thus coding it makes a more efficient use of binary digits; 2) the differential signal has a smaller variance than the original signal, and the quantization noise, which is proportional to the variance of the signal is smaller; 3) for pictorial data the probability density function of the differential signal is more "deterministic like" than the original signals permitting a simpler design of an optimum quantizer. These potentials of the DPCM system have been explored in coding one dimensional signals. A popular DPCM system is one in which each element is predicted using only the adjacent element (element - differential quantization). The one-element DPCM system has been used in coding both monochromatic and color pictures with success [1,2]. Recent results have indicated that the DPCM system can be employed for coding pictorial data more efficiently by designing its predictor such that in addition to horizontal correlations the correlation of the signal in other spatial directions is also utilized [3]. The design of this predictor is simplified by modeling the autocorrelation function of the pictorial data by parametric functions.

It has been established that the most efficient technique of coding color pictures is to code the luminance and the chromaticity components separately. Link et al. [2] have reported good results coding luminance and chromaticity components separately using the element-differential quantization technique. The n^{th} order DPCM system that is being studied uses the correlation of the data in all spatial directions (Figure 3.2-1). This results in a differential signal that is less correlated and has a smaller entropy than the differential signal obtained by utilizing only the horizontal correlations. Coding this signal gives a smaller mean

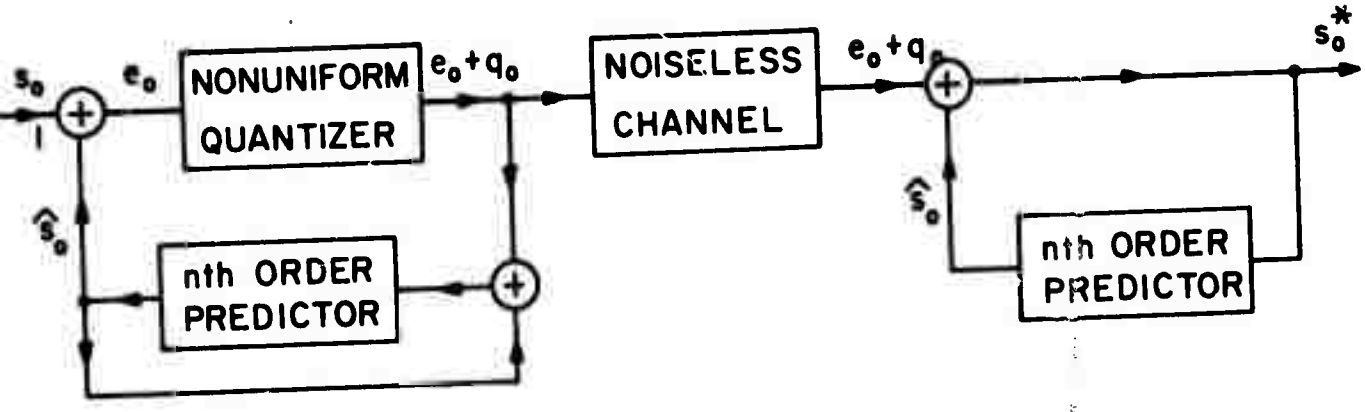

DPCM system

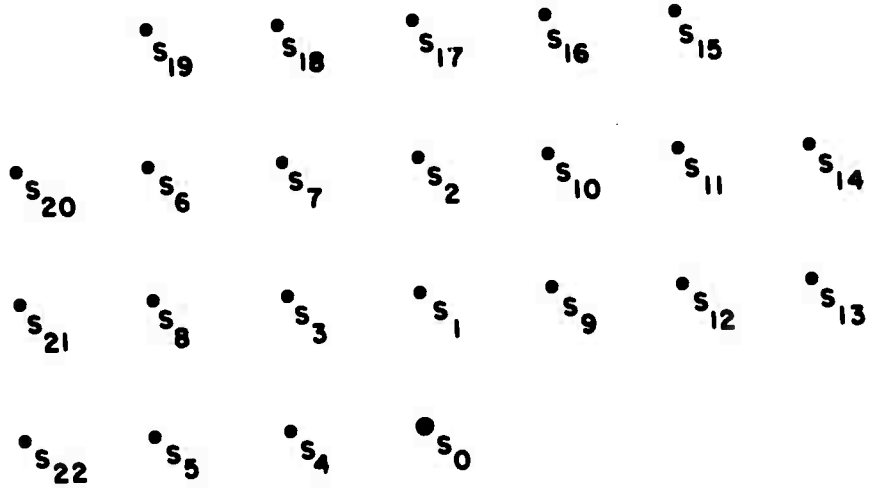

Picture elements employed in predicting S_0.

Figure 3.2-1 Block diagram of differential PCM color image coder.

square error (MSE) than the differential signal in the element-differential quantization system.

The coding efficiency of a DPCM system is improved by using a variable-length coder (Huffman Coder) at the output of the quantizer. This reduces the average bit rate to the entropy of the quantized differential signal. Since in a n^{th} order DPCM system the entropy of the differential signal is smaller than the entropy of the corresponding element-differential quantization system the addition of the variable-length coder results in further improvement of it over the element-differential quantization system.

The results of the above analysis are also used to compare the n^{th} order DPCM system with spatial transform coding of color images [4]. The comparison is based on MSE criterion.

If in a DPCM system (also in a PCM system) a fixed number of binary digits is assigned to encode a given signal, the sampling error may be reduced by increasing the sampling rate. But, this requires coarser quantization of each sample thus increasing the quantization error. In the same manner, finer quantization of each sample means less samples can be quantized. That in turn increases the sampling error. Therefore, there is an optimum rate of sampling and an optimum number of quantization levels that will minimize the total mean square error. For a simple PCM system this problem was explored using pictorial data and the best combination of the sampling rate and the number of quantization levels were specified in terms of the spatial correlation of the data [5]. This problem system is investigated for the DPCM system. The analysis also gives a comparison of the DPCM system with the delta modulation system. Consideration is also being given to some adaptive forms of delta modulation. The interesting feature of the adaptive delta modulators is that the shape of the power spectrum of the coding error can be controlled to some extent. This feature is used in coding color images by shifting a large fraction of

the coding error to the frequency band least objectionable to a human observer.

Most of the work concerned with modeling pictorial data with a random field requires a knowledge of the spatial correlation of the data. In some problems a functional form for the autocorrelation function of the random field is essential where in others this is not necessary though it simplifies the problem. A popular model is a random field with an autocorrelation function

$$R(t_1, t_2) = \exp\left\{ -\alpha |t_1| - \beta |t_2| \right\}.$$

This model implies the pictorial data is a one dimensional Markov process along each line and each column which experimental evidences have shown to be true for most pictures. But this model also implies more correlation in horizontal and vertical directions which is not the case for most pictures. A different model for pictorial data is a random field with an autocorrelation function

$$R(t_1, t_2) = \exp\left(-\sqrt{\alpha^2 t_1^2 + \beta^2 t_2^2 + \nu t_1 t_2} \right).$$

This model eliminates the above shortcoming and experimental results have indicated that it is a more realistic model for natural pictorial data.

The details will be published in an article titled, "DPCM Coding of Color Signals," in the Proceedings of International Telemetering Conference, October 1972.

References

1. J. B. O'Neal, Jr., "Delta Modulation Quantizing Noise Analytical and Computer Simulation Results for Gaussian and Television Input Signals," Bell System Technical Journal, Vol. 45, pp. 117-142, January 1966.

2. J. O. Limb, C. B. Rubinstein, and K. A. Walsh, "Digital Coding of Color Picturephone Signals by Element Differential Quantization," IEEE Transactions on Communication Technology, Vol. COM-19, pp. 992-1005, December 1971.

3. A. Habibi, "Comparison of Nth Order DPCM Encoder with Linear Transformations and Block Quantization Techniques," IEEE Transactions on Communication Technology, Vol. COM-19, pp. 948-956, December 1971.

4. W. K. Pratt, "Spatial Transform Coding of Color Images," IEEE Transactions on Communication Technology, Vol. COM-19, December 1971, pp. 980-991.

5. A. Habibi, P. A. Wintz, "Image Coding by Linear Transformation and Block Quantization," IEEE Transactions on Communication Technology, Vol. COM-19, February 1971.

3.3 Monochrome Transform Image Coding Extensions

Clifford Reader

The implementation of orthogonal transformation over images composed of a large array of pixels can be a significant computational task. An earlier work [1] has shown that, if a degree of error may be tolerated, then the image may be divided into blocks each of which may be separately transformed. Typically, for an image of 256 by 256 pixels, blocks may be selected of size 16 by 16 pixels. The problem which arises is that for high orders of redundancy reduction, the edges of the blocks and the low sequency reconstruction patterns become visible. The object of this study was to minimize this spurious block pattern and checkering effect.

Subsampling Patterns. The desired effect of blurring the edges of the blocks may be attained by spatially subsampling the image prior to dividing it into blocks. Preferably (from the standpoint of blurring edges) this should be done in as random a way as possible. However, the redundancy reduction properties of the transform derive from exploitation of the inter-element correlations, and any subsampling

scheme reduces the correlation between samples in the rearranged array. Thus, there will be a trade-off between the reduction of image quality due to this effect and any improvement due to the elimination of the block pattern and checkering.

The subsampling pattern chosen for evaluation is formed from a Latin square. A Latin square is an n x n array of the integers 1 to n such that each integer appears once and only once in each row and column of the array. The simplest non-trivial example is the 2 x 2 Latin square.

$$\begin{matrix} 1 & 2 \\ 2 & 1 \end{matrix}$$

Repeated over a large array this is equivalent to the checkerboard pattern. Thus the image could be separated into two fields according to the pattern and the 16 by 16 blocks selected from the resultant array. Two examples are shown out of the 24 possible 4 by 4 Latin squares of interest.

(i)
$$\begin{matrix} 1 & 2 & 3 & 4 \\ 2 & 1 & 4 & 3 \\ 3 & 4 & 1 & 2 \\ 4 & 3 & 2 & 1 \end{matrix}$$

(ii)
$$\begin{matrix} 1 & 2 & 3 & 4 \\ 4 & 3 & 2 & 1 \\ 2 & 1 & 4 & 3 \\ 3 & 4 & 1 & 2 \end{matrix}$$

Application of these will of course lead to 4 fields; but the inter-element correlation of each of the fields will be much reduced. The basic scheme may be modified by selecting the elements in sub-blocks of m x m elements (m = 1,2,4,8). This has the advantage that the inter-element correlation will be high across the sub-block but the edges of these sub-blocks will appear just as those of the larger blocks. An investigation was made to determine the statistics of the Latin squares and hence choose those most likely to be of use [2]. From this it was found that Latin square number (i) has the least mean squared error of all the 4 by 4 Latin squares and number (ii) the greatest. However, the difference in expected mean squared error appeared small enough to leave freedom to choose the Latin square most suited to re-ordering the data.

Experimental Results. Results were obtained for the checkerboard pattern and the two Latin square patterns (i) and (ii) for sub-block sizes. The transform domains were quantized by an optimized scheme to give an 8:1 bandwidth reduction for the Hadamard transform and a 12:1 bandwidth reduction for the Karhunen-Loeve transform.

Figure 3.3-1a shows the result of bandwidth reduction without spatial subsampling. The checkering effect is pronounced and the block edges are visible over part of the Karhunen-Loeve transformed image. Figure 3.3-1b presents the results of a checkerboard subsampling of the image. For the Hadamard transform case the checkering effect has been partially replaced by a small overall reduction in density, however, for the Karhunen-Loeve case, the image has been degraded by the subsampling. Figure 3.3-1c presents the results for subsampling with the Latin square patterns. These results are similar to that for checkerboard subsampling, the main difference being variation in the size of the checkering.

Conclusion. There is a modest overall improvement in subjective image quality when spatial subsampling is used with the Hadamard transform owing to minimization of the checkering effect. The visibility of that effect may be controlled by the choice of subsampling patterns. Application of subsampling schemes to the Karhunen-Loeve transform coding of images leads only to a reduction of image quality. Use of a large sub-block size results in the visibility of those sub-blocks and the use of a small sub-block size reduces the effective inter-element correlation and thus the efficiency of the transform. The scheme should yield an improvement in image quality for the sub-optimum Fourier and Slant transforms.

References

1. Pratt, W. K., Andrews, H. C., "Transform Image Coding," USCEE Report 387, March 1970, pp. 56-57.

2. Reader, C., "Spatial Subsampling for Transform Coding of Images," to be published, Proceedings of the Walsh Function Symposium, Washington, D.C., March 1972.

(a)

Hadamard Transform
Mean squared error = 0.161%

Karhunen-Loeve Transform
Mean squared error = 0.181%

No Subsampling

(b)

Reproduced from best available copy.

Hadamard Transform
Sub-block size 8 x 8
Mean squared error = 0.186%

Karhunen-Loeve Transform
Sub-block size 2 x 2
Mean squared error = 0.312%

Checkerboard Subsampling

(c)

Hadamard Transform
Sub-block size 8 x 8
Latin square (i)
Mean squared error = 0.189%

Hadamard Transform
Sub-block size 8 x 8
Latin square (ii)
Mean squared error = 0.182%

Figure 3.3-1. Effect of spatial subsampling for image transform coding.

3.4 Slant Transform Image Coding

Wen-Hsiung Chen, William K. Pratt, Lloyd R. Welch

A desirable property for an image coding transform is that the transform compact the image energy to as few of the transform domain samples as possible. Qualitatively speaking, a high degree of energy compaction will result if the basis vectors of the transformation matrix "resemble" typical horizontal or vertical lines of an image. If one examines the lines of a typical monochrome image, it is found that a large number of the lines are of nearly constant grey level over a considerable length. The Fourier, Hadmard and Haar transforms possess a constant valued basis vector that provides an efficient representation for constant grey level image lines, while the Karhunen-Loeve transform has a nearly constant basis vector suitable for this representation. Another type of typical image line is the line that linearly increases or decreases in brightness over the length. None of the data transforms previously mentioned possess a sawtooth or slant basis vector that efficiently represents such image lines.

With this background an investigation was undertaken to develop an image coding slant transform matrix possessing the following properties:

1. orthogonal set of basis vectors
2. constant basis vector
3. slant basis vector
4. sequency property
5. variable size transformation
6. fast computational algorithm
7. high energy compaction

Slant Transform Construction. For a vector length of N = 2 the slant transform is identical to the Hadamard transform of order two.

$$S_2 = \frac{1}{\sqrt{2}} \begin{bmatrix} 1 & 1 \\ 1 & -1 \end{bmatrix}$$

A slant transform for N = 4 can be written as

$$\left[S_4\right] = \frac{1}{\sqrt{4}} \begin{bmatrix} 1 & 1 & 1 & 1 \\ \frac{3}{\sqrt{5}} & \frac{1}{\sqrt{5}} & \frac{-1}{\sqrt{5}} & \frac{-3}{\sqrt{5}} \\ 1 & -1 & -1 & 1 \\ \frac{1}{\sqrt{5}} & \frac{-3}{\sqrt{5}} & \frac{3}{\sqrt{5}} & \frac{-1}{\sqrt{5}} \end{bmatrix} \tag{6}$$

It is easily shown that S_4 is orthonormal. Further note that S_4 possesses the sequency property; each row has an increasing number of sign reversals from 0 to 3. The fast computational property of S_4 is apparent from the matrix decomposition

$$\left[S_4\right] = \frac{1}{\sqrt{4}} \begin{bmatrix} 1 & 0 & 0 & 0 \\ 0 & \frac{3}{\sqrt{5}} & 0 & 0 \\ 0 & 0 & 1 & 0 \\ 0 & 0 & 0 & \frac{3}{\sqrt{5}} \end{bmatrix} \begin{bmatrix} 1 & 0 & 0 & 0 \\ 0 & 0 & 1 & \frac{1}{3} \\ 1 & -1 & 0 & 0 \\ 0 & 0 & \frac{1}{3} & -1 \end{bmatrix} \begin{bmatrix} 1 & 0 & 0 & 1 \\ 0 & 1 & 1 & 0 \\ 1 & 0 & 0 & -1 \\ 0 & 1 & -1 & 0 \end{bmatrix} \tag{7}$$

The total computational requirements are 8 adds and 6 multiplies. For purposes of comparison a fourth order Hadamard transform requires 8 adds and 4 multiplies. The construction for slant matrices of order N from slant matrices of order N/2 is given by

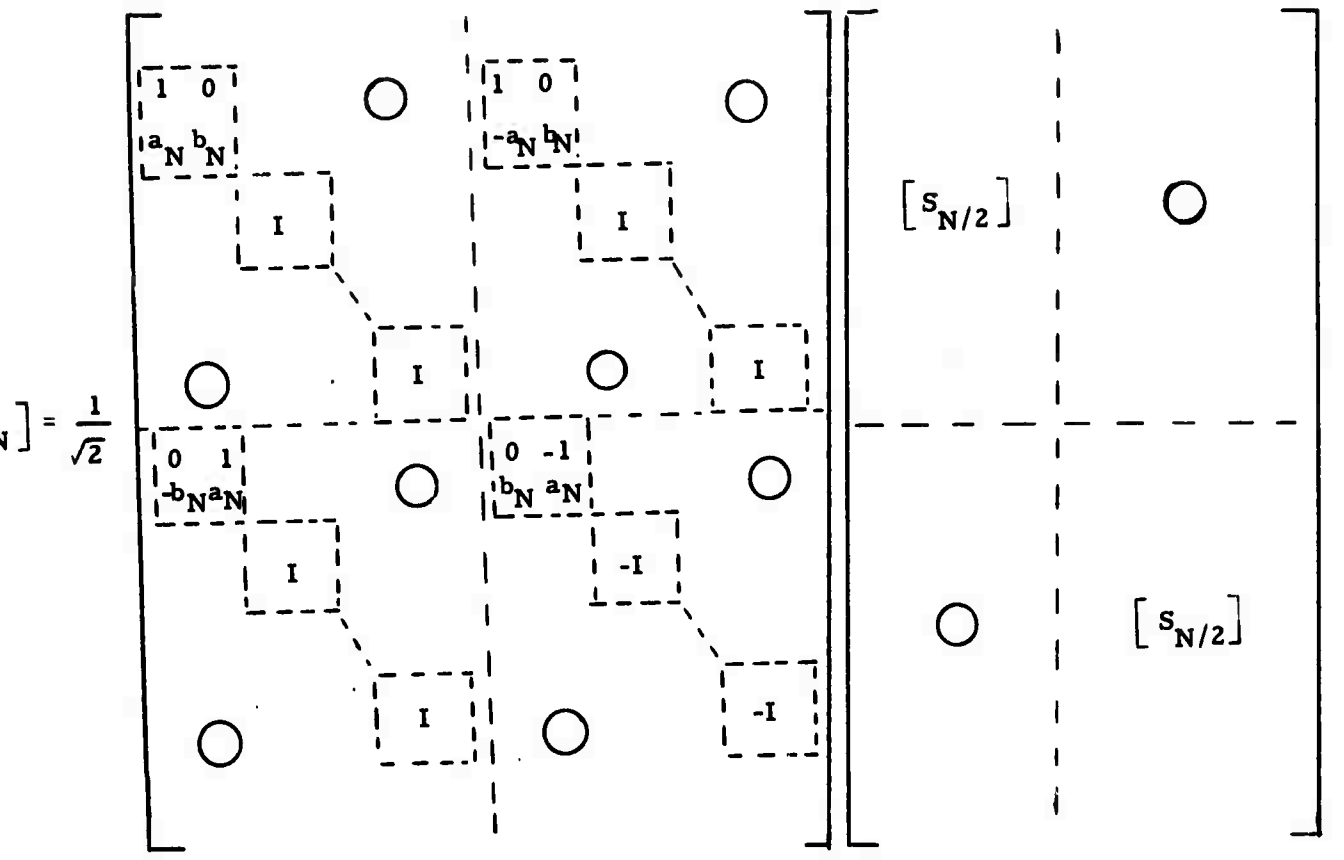

where I represents a 2 x 2 identity matrix and a_N, b_N are constants.

Slant Transform Image Coding. Let $[f(x, y)]$ represent the brightness samples of an N by N element image. The two dimensional Slant transform of the image is given by

$$[F(u, v)] = [S_N][f(x, y)][S_N]^T$$

In effect, the pre-multiplication of $[f(x, y)]$ by $[S_N]$ performs a one dimensional slant transform of each column of the image matrix, and the post-multiplication by $[S_N]^T$ performs a one dimensional transform of the rows of the image.

A bandwidth reduction can be obtained with the Slant transform by efficiency quantizing each transform domain sample.

A statistical evaluation of the coding performance of the slant transform has shown that it provides almost as small a mean square error as the optimum Karhunen-Loeve transform (which does not possess a fast algorithm), and a lower error than the Hadamard transform. Figure 3.4-1 contains reconstructions of Slant, Hadamard and Karhunen-Loeve transform coded image reconstructions coded with an average of 15. bits per pixel. Subjectively, the quality of the Slant coded image is superior to the Hadamard coded image.

Reference

1. W. K. Pratt, L. R. Welch, and W. Chen, "Slant Transforms for Image Coding," Proceedings Symposium on Applications of Walsh Functions, March, 1972.

3.5 Color Image Transform Coding

William K. Pratt

Digital image transforms have been applied quite successfully to obtain a bandwidth reduction and tolerance to channel errors for monochrome images. The potential for monochrome image bandwidth compression with transform coding arises from the spatial correlation within natural images. As a result of this spatial correlation, the image energy within the transform domain tends to be clustered toward a relatively few number of transform samples. Low magnitude samples may either be discarded completely or coded with a few number of bits without seriously effecting image quality. Sample reductions on the order of 5:1, compared to conventional PCM coding, have been reported for transform coding of monochrome images.

Preliminary studies have indicated that the spatial redundancy of

(a) Hadamard

(b) Slant

(c) Karhunen-Loeve

Figure 3.4-1. Hadamard, Slant, and Karhunen-Loeve image coding.

Reproduced from best available copy.

color images and the limitations of human color vision can be exploited by transmission of color television and facsimile. Figure 3.5-1 contains a block diagram of a color image transform coding system. In the system the color image is represented by three source tristimulus signals $R(x, y)$, $G(x, y)$, $B(x, y)$ that specify the red, green, and blue content of an image element at coordinates (x, y). The source tristimulus signals are then converted to a new three dimensional space through some linear or non-linear, invertible coordinate conversion process. The objective of the coordinate conversion is to produce three planes of data, $f_1(y, y)$, $f_2(x, y)$, $f_3(x, y)$, to be called color signals, that are most amenable to transform coding. Next, a spatial, unitary transformation is performed on each color signal plane resulting in three transform domain planes $F_1(u, v)$, $F_2(u, v)$, $F_3(u, v)$. The Fourier, Hadamard, and Karhunen-Loeve transforms have been investigated for the spatial transformation. Quantization and coding to achieve a bandwidth reduction is then performed on the three transform domains. At the receiver, the channel output is decoded, and the inverse spatial transforms and inverse coordinate conversion operations are performed to reconstruct the source tristimulus signals.

In order to optimally design the color image transform coder of Figure 3.5-1, it is necessary to specify some analytic measure of color image fidelity. Unfortunately, there are no accepted color image fidelity standards. For this reason, the analytic design procedure, adopted for the color image transform coder, has been to select the combination of the color coordinate conversion matrix and spatial, unitary transform matrices to provide the greatest compaction of image energy into the fewest transform domain samples. The coordinate conversion provides the energy compaction between color planes, and the spatial, unitary transforms provide the energy compaction within the color planes. Then the quantization law is selected to minimize the mean square error

$$\mathcal{E}_f^2 = \frac{1}{3N^2} \sum_{k=1}^{3} E\left\{ \left[f_k(x, y) - \hat{f}_k(x, y) \right]^2 \right\}$$

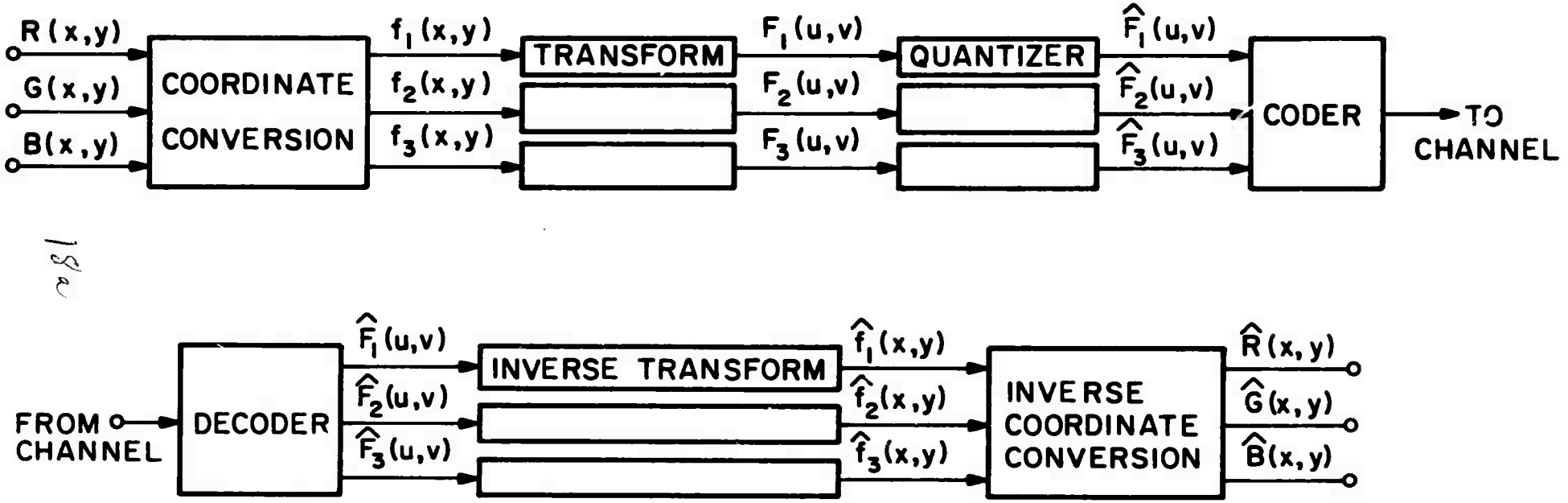

Figure 3.5-1. **Color Image Transform Coding System**

of the color signal planes.

The energy compaction properties of the linear color conversion matrix have been statistically evaluated for the color coordinate systems listed in the tables given below.

Color Coordinate System	Percentage of energy in plane:		
	f_1	f_2	f_3
R G B	33.2	36.2	30.6
U V W	10.4	25.9	63.7
Y I Q	93.0	5.3	1.7
K_1 K_2 K_3	94.0	5.1	.9

As expected from the theoretical considerations the Karhunen-Loeve coordinate system ($K_1K_2K_3$) provides the best energy compaction, while the worst system is the source tristimulus system (RGB). The U. S. standard system for television transmission (YIQ) provides a very good energy compaction. The energy compaction properties of spatial, unitary transforms has been well established. It is known that the Karhunen-Loeve transform provides the greatest degree of energy compaction, followed by the Fourier, and then the Hadamard transforms, but there is relatively little difference between transforms on this basis.

A series of experiments has been performed to subjectively determine the performance of the color image transform coding system using: a) various linear and nonlinear color coordinate systems; b) the Fourier, Hadamard, and Karhunen-Loeve spatial transforms; c) limitations in data block size; and, d) different quantization and coding techniques. Summarizing, the experimental results indicate that:

a) It is preferable to transform code the (Y I Q) color coordinates rather than the (R G B) coordinates of an image.

b) Substantial low pass filtering can be performed on the chromaticity components of a color image without noticeable effect on resolution. There is some color desaturation caused by the low pass filtering, but a linear masking operation can be employed to correct for color shifts. About 0.75 bits per elements are required for chromaticity information.

c) With a hybrid coding scheme using a 16 x 16 element Karhunen-Loeve transform for the luminance signal and 16 x 16 Hadamard transforms for the (I Q) signals, a color image can be coded with only 1.75 bits per element. Preliminary studies indicate that such a system could be implemented for operation approaching real time rates.

Reference

1. W. K. Pratt, "Spatial Transform Coding of Color Images," IEEE Transactions on Communication Technology, Vol. COM-19, No. 9, Part I, December, 1971, pp. 980-992.

3.6 Effect of Channel Errors for PCM Color Image Transmission [1,2]

William K. Pratt

In the transmission of color images over digital communication links, consideration must be given to the effect of errors in the reconstructed images as a result of receiver noise. The general solution to this problem is many faceted: it depends on the type of images to be transmitted and their use; the error criterion; the methods of source and channel coding; and the statistical model for the communication channel. Consideration here is given to the practical case of color image transmission over a binary symmetric channel (BSC) for color images represented by the standard three color primary system. Constant word length pulse code modulation (PCM) coding is assumed for each primary signal.

No source coding for redundancy removal nor channel coding for error correction is considered.

Figure 3.6-1 contains models for the analysis of color image transmission errors. Two cases have been considered: transmission of tristimulus values ($T_1 T_2 T_3$) of a color and transmission of the luminance (Y) and chromaticities ($t_1 t_2$). In the tristimulus transmission system the source signals (RGB) normalized to [0, 1], are linearly converted to a set of transmission tristimulus values ($T_1 T_2 T_3$). Each tristimulus component is linearly quantized over its maximum and minimum range to a binary number between 0 and $2^N - 1$ where N is the number of bits allotted to the component. At the receiver an inverse scaling reconstructs the channel error corrupted tristimulus values ($T_1' T_2' T_3'$) which are then converted to red, green, and blue (R' G' B') tristimulus values. As a result of channel errors the values of (R' G' B') may be greater than unity or less than zero. Such values correspond to "colors" that are not physically reproducible. Hence, it is necessary to pass (R' G' B') through limiters to obtain the display tristimulus values (R"G"B"). The color shift between the transmitted color specified by (RGB) and the displayed color given by (R"G"B") is measured in terms of the (Yuv) coordinate system in which Y represents the luminance and u, v are the chromaticities of the color in the Uniform Chromaticity Scale coordinate system. The luminance and chromaticity of a displayed color are given by

$$Y'' = \lambda_1 R'' + \lambda_2 G'' + \lambda_3 B''$$

$$u'' = \frac{\eta_1 R'' + \eta_2 G'' + \eta_3 B''}{\eta_4 R'' + \eta_5 G'' + \eta_6 B''}$$

$$v'' = \frac{\eta_7 R'' + \eta_8 G'' + \eta_9 B''}{\eta_4 R'' + \eta_5 G'' + \eta_6 B''}$$

where λ_k and η_k are coordinate conversion constants.

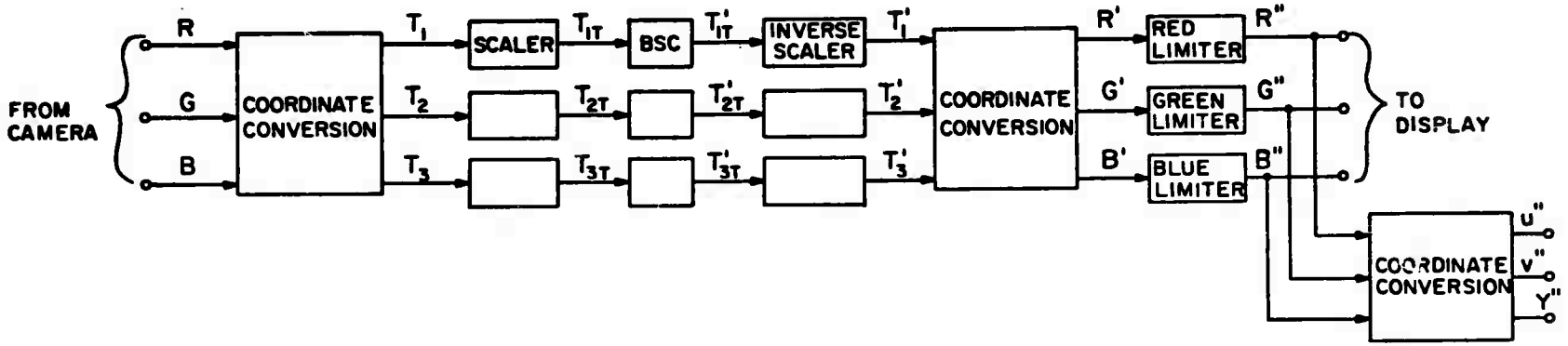

(a) T_1, T_2, T_3 TRANSMISSION

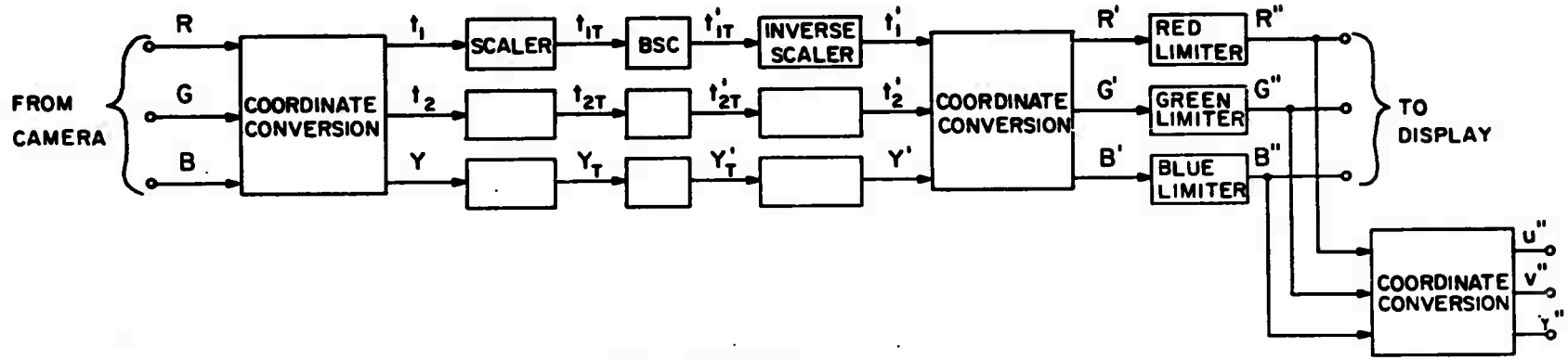

(b) Y , t_1 , t_2 TRANSMISSION

Figure 3.6-1. Models for analysis of channel errors

In analyzing the effects of channel errors or color transmission, the prime interest is the expected color shift and the variance of the color shift, rather than the average color of an image point. Thus, the statistics of interest are the conditional moments of u", v", Y" given that a particular color was transmitted. The nth conditional moment of the display luminance is

$$E\{(Y'')^n|m\} = \sum_{T'_{1T}=0}^{2^N-1} \sum_{T'_{2T}=0}^{2^N-1} \sum_{T'_{3T}=0}^{2^N-1} \left[Y''\left\{T'_{1T}, T'_{2T}, T'_{3T}\right\}\right]^n \cdot P\left\{T'_{1T}|T_{1T}\right\} P\left\{T'_{2T}|T_{2T}\right\} P\left\{T'_{3T}|T_{3T}\right\}$$

The conditional distribution of each channel is given by

$$P\left\{T'_{iT}|T_{iT}\right\} = p^{\left[N-M\left\{T'_{iT}, T_{iT}\right\}\right]} (1-p)^{M\left\{T'_{iT}, T_{iT}\right\}}$$

where p is the probability of a bit error and $M\left\{T'_{iT}, T_{iT}\right\}$ represents the number of bit matches between T'_{iT} and T_{iT}. The remaining conditional moments for u" and v" are found by similar expressions.

Using the preceding analysis the luminance and chromaticity shift have been predicted for several color coordinate transmission systems. Figure 3.6-2 illustrates the chromaticity shifts for the (RGB) and (Yuv) systems. The tail of each arrow represents the transmitted color and the arrowhead denotes the expected value of the received color. Computer simulation experiments have been performed to verify the analytic predictions. In summary, it has been found that the least image degradation occurs for transmission of the (RGB) tristimulus values. In this case the mean color shift is toward a mid-grey. For all other color coordinate transmission systems the color shift is away from grey to a primary complimentary color.

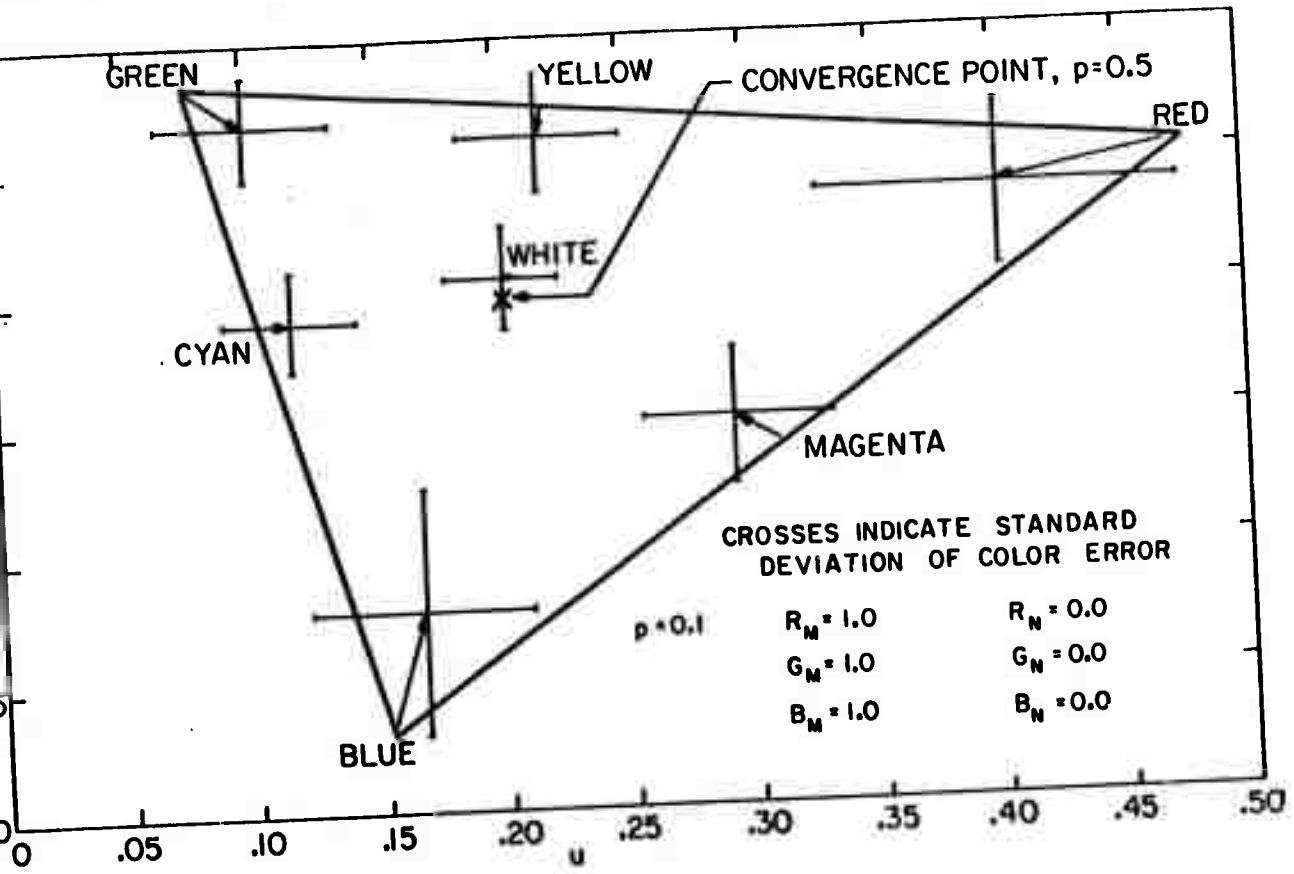

CHROMATICITY SHIFT FOR R,G,B TRANSMISSION

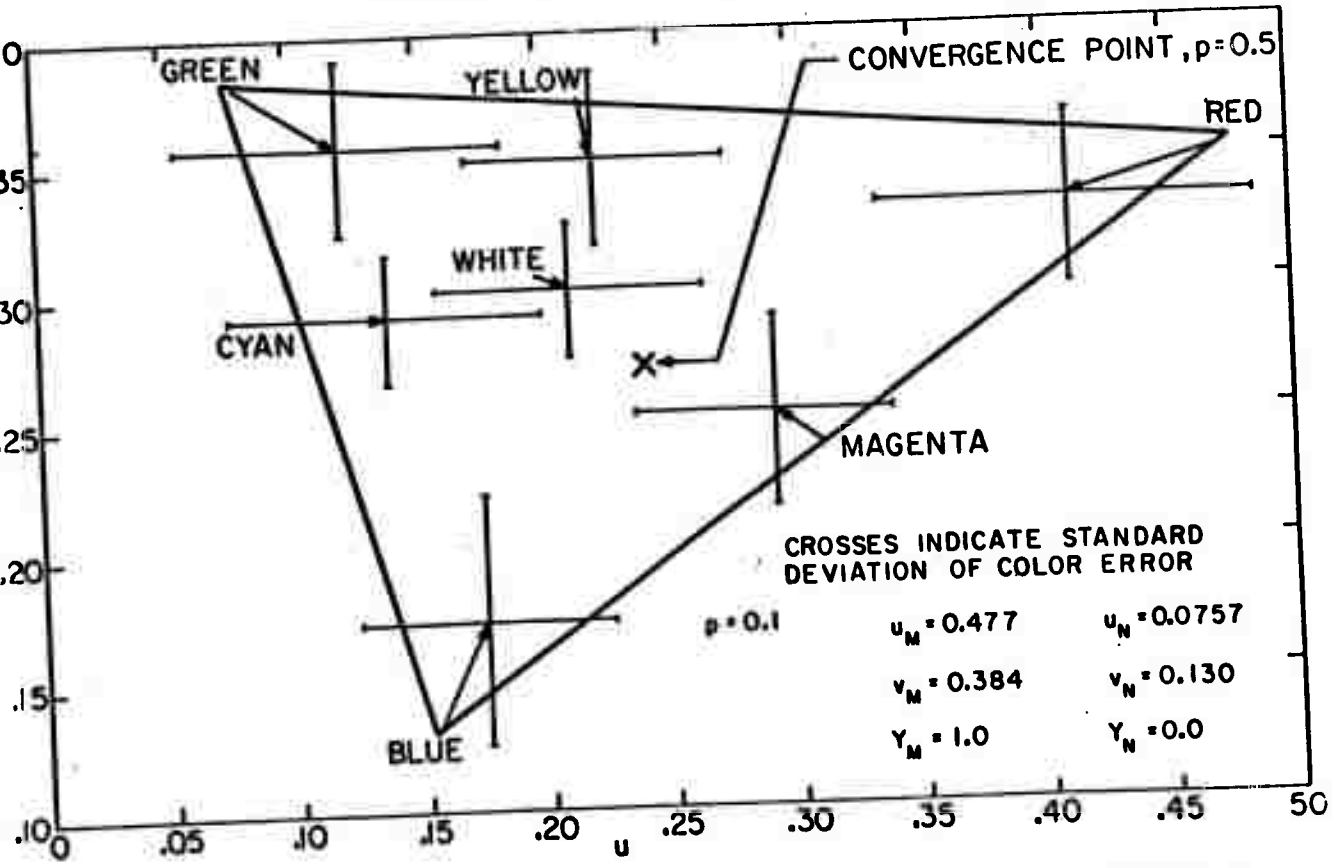

CHROMATICITY DIAGRAM FOR Y,u,v TRANSMISSION

Figure 3.6-2. Chromaticity shift for RGB and Yuv color image transmission systems.

References

1. W. K. Pratt and J. P. Hong, "Effects of BSC Channel Errors on PCM Color Image Transmission," 1970 National Telemetering Conference, April 1970.

2. W. K. Pratt, "Binary Symmetric Channel Error Effects on PCM Color Image Transmission," IEEE Transactions on Information Theory (to be published), 1972.

4. Image Enhancement and Restoration

The use of digital computers for picture "improvement" has been brought to public attention in recent years by their applications in space imagery and biomedical research. The generality and versitility afforded by the general purpose computer provide for innovation in manipulating images for both restoration and enhancement purposes. Image restoration, as defined here, signifies the reconstruction of an image according to some mathematical model to as close to the original as is possible. Typical of such restoration techniques are correction of defocus, motion blur, atmospheric turbulence, etc. Image enhancement is the manipulation of pictorial data for improvement in presentation to a human viewer. Typical of these techniques are high frequency emphasis, contrast improvement, and use of pseudocolor.

The research effort in the last six months has been devoted to a variety of enhancement and restoration tasks. These tasks include studies to determine the applicability of recursive est ation techniques, which have proven highly successful for one dimensional communication problems, to image restoration. Investigations have begun on computer methods of image resolution improvement, image blur compensation, and image noise removal. Also, preliminary studies have been initiated on problems of color image restoration and the use of pseudocolor image enhancement techniques.

4.1 Application of Recursive Estimation to Image Restoration

N. E. Nahi and A. Habibi

In many degraded images the image distortion can be characterized by a random process (noise) with known statistics. Furthermore, in certain applications, the a priori knowledge of the image itself is only of statistical nature.

Image restoration subject to the above restrictions, describes the

classical problem of statistical estimation and filtering, where one basically attempts to filter out the noise from an observation. The most general and computationally efficient procedure available at present to perform this filtering is the recursive estimation methods of Kalman filtering and their nonlinear extensions. However, here it is necessary that the observation be a function of one independent variable, such as time, in contrast with an image which is defined on a plane. During the last year two methods of image restoration based upon the application of recursive estimation have been developed. These methods are very briefly outlined below.

First Method. The statistical information of the image and the noise are assumed to be available in terms of the mean and the two dimensional auto-correlation functions of the signal and noise. The random process representing the image and the noise are assumed wide-sense stationary. Furthermore, it is assumed that the noise is additive. The observation is obtained by horizontal scanning with uniform speed, producing the scanner output $s(t)$, where t represents the time variable. Due to the assumed additive property of the noise, the scanner output $s(t)$ can be decomposed into functions $s_I(t)$ and $s_N(t)$ where the subscripts I and N represent the image and noise respectively and

$$s(t) = s_I(t) + s_N(t) . \qquad (1)$$

The signal $s(t)$ may be vector valued representing vector scanning, i.e., the process of scanning more than one picture line at a time. The required steps for the design of the image enhancer are outlined below:

1. Determine the autocorrelation function of $s_I(t)$ and $s_N(t)$ utilizing the spatial autocorrelation functions of the image and noise.

2. Determine the dynamic (difference equation) models of $s_I(t)$ and $s_N(t)$.

3. Design the appropriate recursive estimator utilizing the above dynamic models.

Due to the periodic nature of the scanner operation, the random process $s_I(t)$ and $s_N(t)$ are in general non-stationary. Determination of dynamic models for such processes is very complex and procedures exist only for some special cases. Often such dynamic systems may not exist at all. Consequently, procedures were developed to determine dynamic models representing approximately the statistics of $s_I(t)$ and $s_N(t)$. The detailed results will appear in a paper titled "Bayesian Recursive Image Estimation," scheduled for publication in IEEE Transactions on Computers, July 1972. The validity of the method is demonstrated here by means of Figure 4.1-1. Photographs (a) and (c) represent the image of a square contaminated by white noise with signal-to ratios of 7.1/3 and 7.1/10. Photographs (b) and (d) represent the estimate.

Second Method. Any monochromatic image can be modeled by specifying its value (gray level) $x(t_1, t_2)$ at each spatial coordinate (t_1, t_2). An ensemble of such images can be modeled by interpreting $x(t_1, t_2)$ as a random field. A class of images with a particular spatial correlation can be modeled by a random field with the same autocorrelation function. When spatial factorization in two dimensions is possible, the autocorrelation function of a random field is related to the transfer function of a system that generates the random field from a set of uncorrelated variates. Then, specifying a class of images by their autocorrelation function specifies a dynamic model representation of these images.

Experimental evidence indicates that random fields with exponential autocorrelation functions are realistic models for a variety of pictorial data. The dynamic model for this random field is a first order partial difference equation in spatial variables. This dynamic model is used to realize a two dimensional recursive filter that gives a linear least mean square error estimate of the random field when a noisy observation is

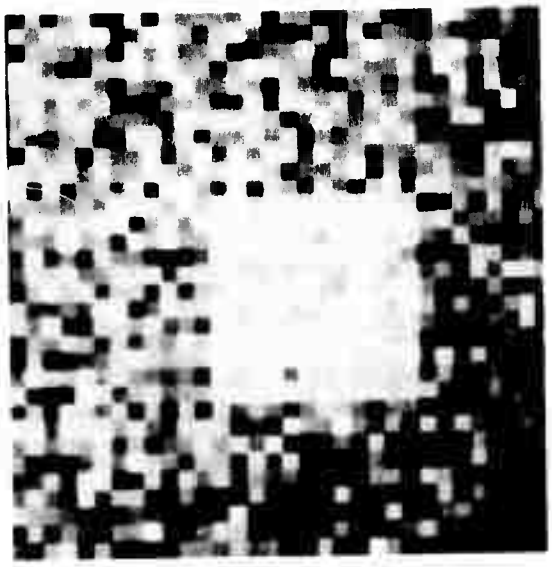

(a) Original

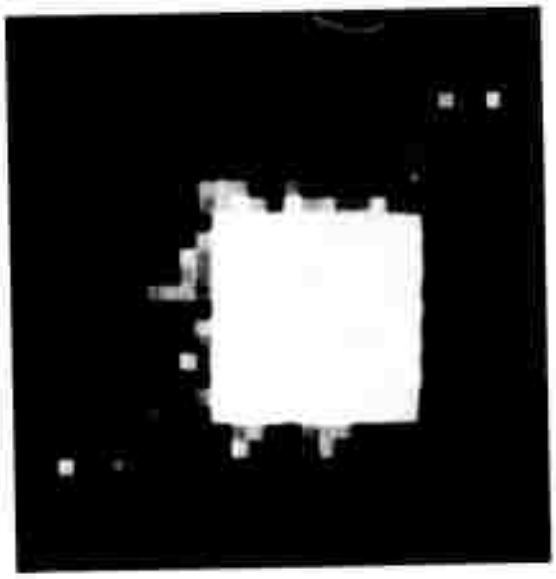

(b) Estimate

Observation and estimates for $\sigma_N^2 = 9$

Reproduced from best available copy.

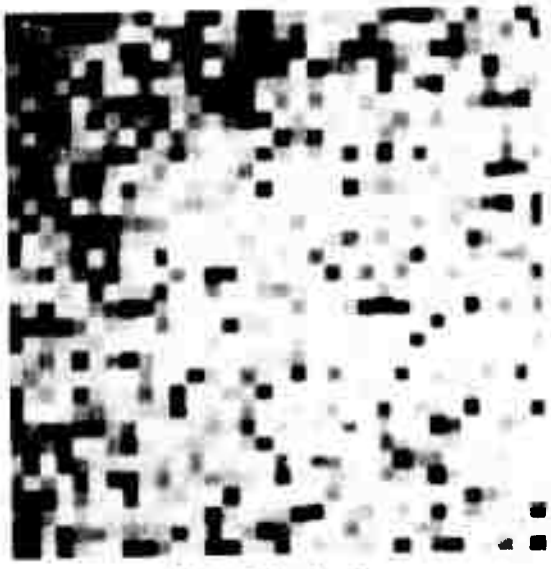

(c) Original

(d) Estimate

Observation and estimates for $\sigma_N^2 = 100$

Figure 4.1-1. Recursive image estimation - first method

used at its input. It is assumed that the noise is white, additive, and uncorrelated with the signal.

The result of this analysis is used to enhance several binary pictures shown in Figure 4.1-2. In each case the picture is contaminated by white noise with a signal-to-noise ratio of 7.1/3.

The estimation technique is generalized to other autoregressive sources. The details will appear in a paper titled, "Two Dimensional Bayesian Estimate of Images," scheduled for publication in IEEE Proceedings, July 1972.

4.2 Restoration of Motion-Degraded Images

Alexander A. Sawchuk

In general, imaging systems such as cameras and television produce recordings of the intensity functions of objects in the field of view. Whenever there is relative motion between the imaging system and object during exposure, the recorded image is degraded and blurred by motion. Recently, there has been a great deal of interest in a posteriori techniques for enhancing motion-degraded blurred images. With improvements in optical systems and recording materials, motion degradation is often the limiting resolution factor in photography by spacecraft and aerial vehicles.

Since the study of motion effects has received relatively little attention in the past, a detailed general mathematical model has been developed which exactly describes motion effects in two dimensional linear incoherent optical systems. Given a mathematical description of any relative movement between vector object coordinates $\underline{u}$ and image coordinates $\underline{x}$, a response function $h(\underline{x}, \underline{u})$ can be derived [1], [2]. The function gives the image as a function of $\underline{x}$ due to a unit object impulse at $\underline{u}$, and contains all the motion degradation effects. The most general linear transformation from object intensity function $O(\underline{u})$ to image intensity $I(\underline{x})$ is then given by a superposition integral

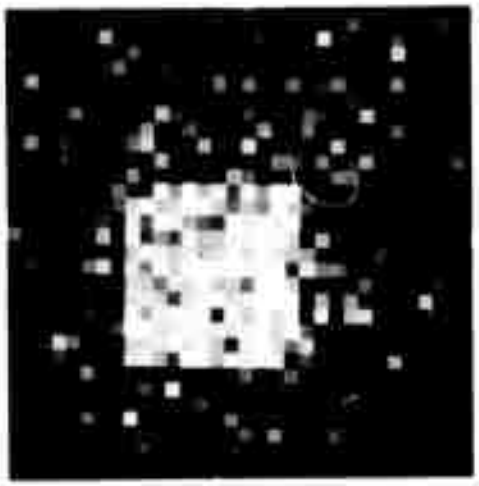

(a) Noisy Signal

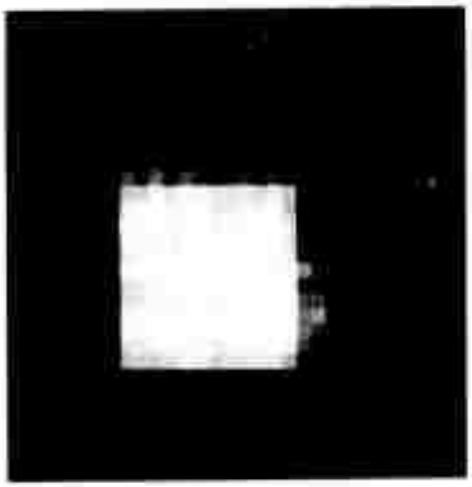

(b) Filtered Signal

(c) Noisy Signal

(d) Filtered Signal

Reproduced from best available copy.

(e) Noisy Signal

(f) Filtered Signal

Figure 4.1-2. Recursive image estimation - second method

$$I(\underline{x}) = \int_{-\infty}^{\infty} h(\underline{x}, \underline{u})\, O(\underline{u})\, d\underline{u} \qquad (4.2\text{-}1)$$

over the entire object. The form of $h(\underline{x}, \underline{u})$ generally varies with the position of the object impulse $\underline{u}$, and is called a space-variant point-spread function in the context of image processing. If $h(\underline{x}, \underline{u})$ can be written as a function only of the difference $\underline{x}-\underline{u}$, then $h(\underline{x}, \underline{u})$ is space-invariant and equation (4.2-1) simplifies to a convolution. Previous work in the motion problem has been limited almost exclusively to the space-invariant case. In most practical cases of aerial imaging, space-invariant motion blur occurs only when the object intensity plane and film plane are parallel--the case when the camera points straight down while moving. This is almost never realized in practice, so that the degradation in aerial imaging is almost always space-variant. The system analysis of motion blur reduces the degradation to a standard form and yields insight into the problem of restoration in the space-invariant cases.

A fundamental example of motion blur occurs when the object is moving at constant velocity V during the fixed exposure time interval $[0, T]$. The recorded image I(x) is formed by the time integration

$$I(x) = \int_{0}^{T} I(x, t)\, dt$$

of the moving image $I(x, t)$ over the exposure interval. In the constant velocity case, $I(x, t) = O(x-Vt)$, and substitution into the above equation gives

$$I(x) = \int_{u=x-Vt}^{u=x} \frac{O(u)\, du}{V}$$

as the expression for the image. From this expression the system point-spread function is identified as

$$h(u) = \begin{cases} \frac{1}{V} & 0 \leq u \leq VT \\ 0 & \text{elsewhere} \end{cases}$$

which is space-invariant since all points in the object follow the same path. Photograph (a) of Figure 4.2-1 contains a uniformly illuminated square object function and Photograph (b) is a computer simulated image of the object blurred by constant velocity motion. The blur is visible only at the edges of the recorded image because the object is uniformly illuminated. However, the general method applies to gray scale imaging where blurring is visible over the entire field.

A more complex type of motion blur occurs in the case of aerial photography by a moving system oriented at an oblique angle with respect to the ground. The motion blur for this geometry is expressed by a space-variant operation; the motion of object points in the imaging system varies over the field. The object is not only blurred, but is geometrically distorted by the imaging system. Photograph (c) is a simulation of a square imaged by a camera moving at constant altitude over the ground, with constant velocity toward the direction of movement at an angle $\phi=20^{o}$ from vertical. The visible blurring on the top and bottom edges varies with position. Photograph (d) shows the square imaged by a camera moving in the same way, except that the camera looks sideways at an angle $\beta = 20^{o}$ from vertical. A simple physical example of side oblique blurring occurs when a photograph is taken from a moving car. The points farther off in the field are blurred much less than those close to the camera.

A wide variety of enhancement, restoration, and statistical techniques are available for image processing, but to date few of them have been applicable or of practical use when the degradation is space-variant. When no noise is present in the space-invariant case, inverse filters in the Fourier domain are useful for restoration. Photograph (e)

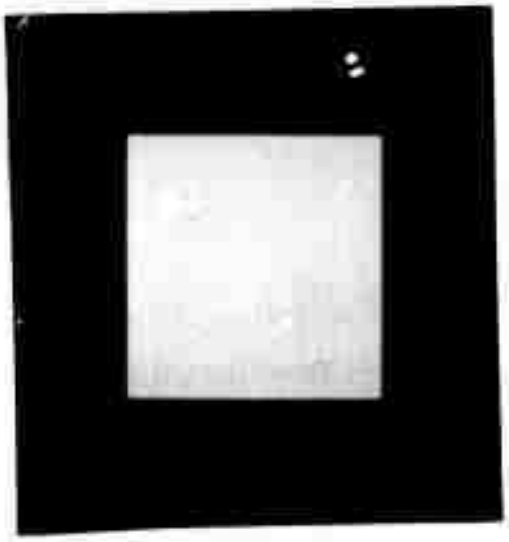

(a) Uniformly illuminated square

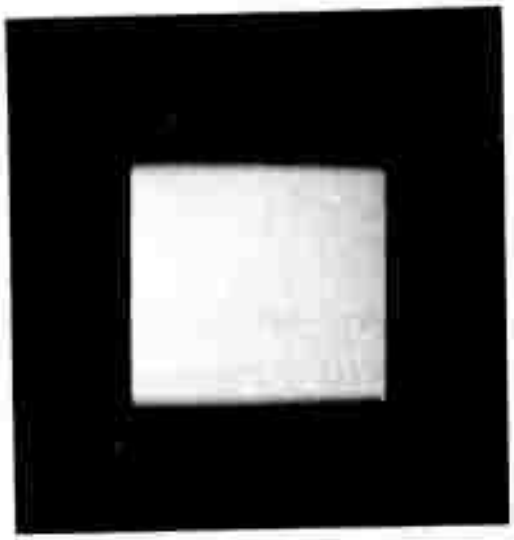

(b) Square blurred by constant velocity motion

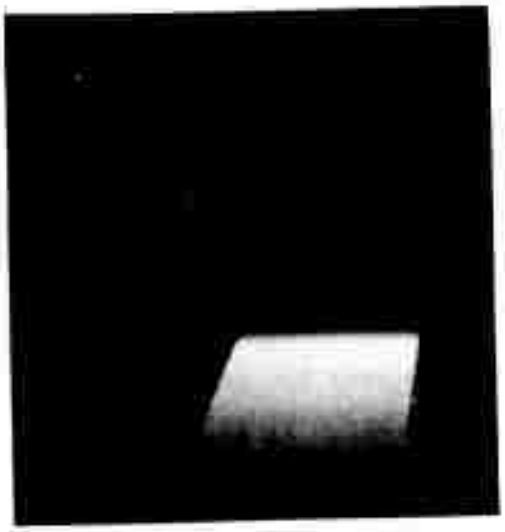

(c) Square blurred by moving forward oblique camera

Reproduced from best available copy.

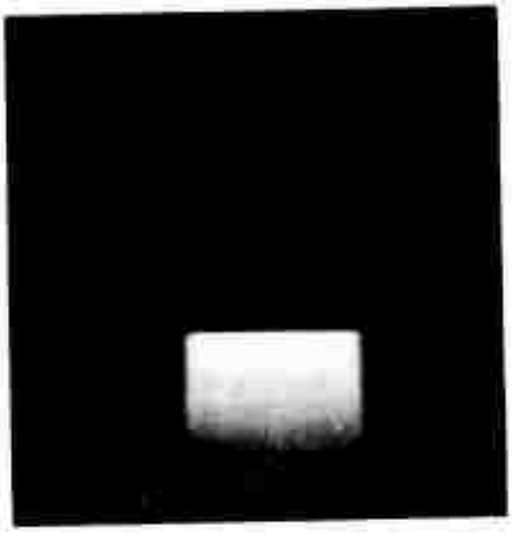

(d) Square blurred by moving side oblique camera

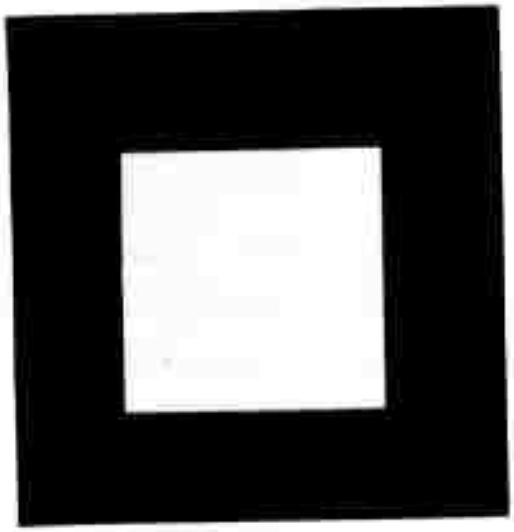

(e) Restoration of constant velocity motion blur

is obtained by dividing the Fourier transform of the blurred Photograph (b) by the transform of the constant velocity blur, and inverse transforming the result to produce the restored image. The resultant image is nearly identical to the original object function.

Unfortunately, inverse filtering is not directly applicable when the blur is space-variant. However, for a large class of moving systems, especially aerial systems, it is possible to decompose the overall space-variant operation into an equivalent cascade of a space-invariant system $h(\underline{x}, \underline{u})$ and a time independent fixed geometrical distortion, as shown in Figure 4.2-2. Decomposing the system in this way immediately reveals the solution to the restoration problem. The geometrical distortion is fixed in time and can be inverted in the recorded $I(\underline{x})$ to produce an intermediate image. Then, the intermediate image can be processed by an inverse filter to give an estimate of $O(\underline{u})$. Thus it is possible to convert the forward and side oblique blurred images to the equivalent space-invariant blur of Photograph (b), and inverse filtering then gives the restoration of Photograph (e). The method is extendable to restore images blurred by cameras at fixed altitudes and orientation traveling with any known motion over the object plane. When noise is present, space-invariant statistical filters can be used in place of the inverse filters. Some advantages of this method are its applicability to a large general class of motion blurred images and its ease in practical implementation.

A number of related methods for space-variant restoration also seem promising. The Mellin transform is a special case of space-variant decomposition useful in restoring degradations by certain types of motion and optical aberrations [1]. Future research will be directed at studying other types of space-variant decomposition and determining the applicability of these techniques to general problems of image restoration in the noisy and noise-free case.

Portions of this work will appear in the Proceedings of the IEEE

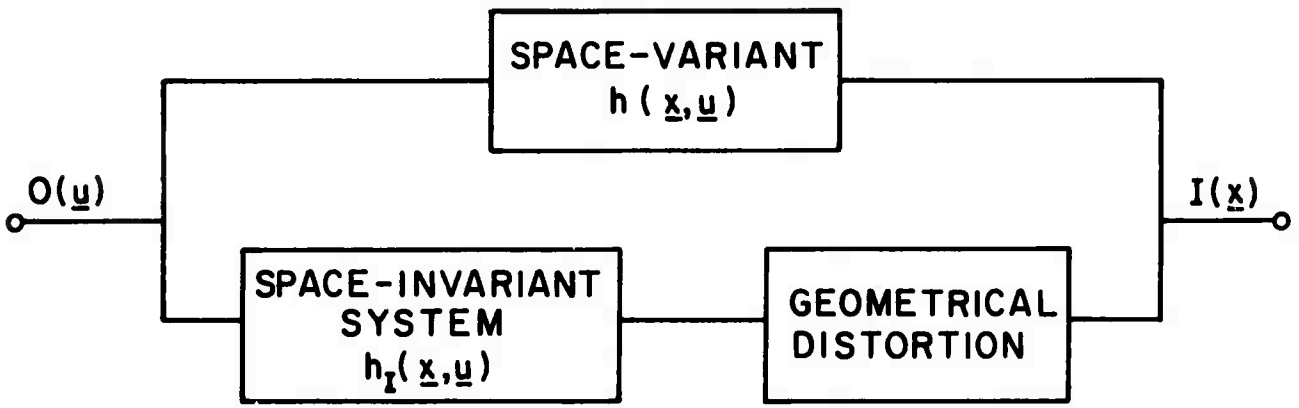

Figure 4.2-2 Space-Variant Decomposition

[2] and will be presented at the Spring Convention of the Optical Society of America.

References

1. Sawchuk, A. A., "Space-Variant Motion Degradation and Restoration," Ph.D. Dissertation, Department of Electrical Engineering, Stanford University, Stanford, California (1972).

2. Sawchuk, A. A., "Linear Space-Variant Motion Degradation and Restoration," Proceedings of the IEEE, 60, July 1972, (to appear).

4.3 Superresolution Image Restoration*

Harry C. Andrews, Anil K. Jain

Superresolution image restoration by the technique of analytic continuation is based upon some academically intriguing principles that have yet to be demonstrated for practical use in general two dimensional image formats. To date studies of analytic continuation for resolution improvement beyond the classical diffraction limit have been limited to one dimensional signals [1,2] and a very few two dimensional noise free examples [3]. This research is directed toward the determination of the usefulness of the theory of analytic continuation to the restoration of two dimensional imagery.

Basically, the motivation behind the use of analytic continuation is to "continue" the known object spectrum beyond the diffraction limit of the imaging system. This requires prior knowledge of the space limited object, say within the range of -A, A and -B, B. Outside this range the object function $o(x, y)$ is assumed zero. Furthermore, it is assumed that the object passes through some space invariant imaging system with impulse response $h(x, y)$ resulting in an image function given by

*Portions of this research were sponsored by the National Science Foundation (NSF-GK-20258).

$$i(x,y) = \int_{-\infty}^{\infty}\int o(\xi,\eta)\, h(x-\xi,\, y-\eta)\, d\xi\, d\eta$$

Taking the two dimensional Fourier transforms of the image function, object function, and impulse response one obtains

$$I(u,v) = \frac{1}{4\pi^2} \int_{-\infty}^{\infty}\int i(x,y) \exp\{j(ux+vy)\}\, dx\, dy$$

$$O(u,v) = \frac{1}{4\pi^2} \int_{-A}^{A}\int_{-B}^{B} o(x,y) \exp\{j(ux,vy)\}\, dx\, dy$$

$$H(u,v) = \frac{1}{4\pi^2} \int_{-\infty}^{\infty}\int h(x,y) \exp\{j(ux+vy)\}\, dx\, dy$$

The image spectrum is then given by

$$I(u,v) = O(u,v)\, H(u,v) \quad \text{for} \quad |u|, |v| \leq \infty$$

But for a purely diffraction limited imaging system

$$H(u,v) = 0 \begin{cases} |u| \geq \Omega/2 \\ |v| \geq w/2 \end{cases}$$

In the subsequent analysis, for simplicity, it will be assumed that $H(u,v)$ equals unity over its pass band.

It is possible to expand the object spectral function into a series of complete orthogonal functions $\{\psi, \Phi\}$ as

$$O(u,v) = \sum_{m=0}^{\infty}\sum_{n=0}^{\infty} a_n b_m \psi_n(u)\, \Phi_m(v) \qquad (4.3\text{-}1)$$

where a_n and b_m are the appropriate weighting coefficients. Then integrating over the diffraction band gives

$$\int_{-\Omega}^{\Omega/2}\int_{-w/2}^{w/2} O(u,v)\,\psi_k(u)\,\Phi_\ell(v)\,du\,dv = \sum_{m=0}^{\infty}\sum_{n=0}^{\infty} a_n b_n \int_{-\Omega/2}^{\Omega/2} \psi_k(u)\,\psi_m(u)\,du \int_{-w/2}^{w/2} \Phi_\ell(v)\,\Phi_n(v)\,dv \qquad (4.3\text{-}2)$$

Now let the functions $\{\Phi, \psi\}$ be the set of prolate spheroidal wave functions (PSWF) that are orthogonal on the closed interval as well as the real line [4]. Then

$$a_n b_m = \frac{1}{\lambda_n^{(u)}\,\lambda_m^{(v)}} \int_{-\Omega/2}^{\Omega/2}\int_{-w/2}^{w/2} O(u,v)\,\psi_n(u)\,\Phi_m(v)\,du\,dv$$

where the λ's are the eigenvalues of the integrals in the right hand portion of equation (4.3-2). The object function is then obtained by the inverse Fourier transform.

$$o(x,y) = \int_{-\infty}^{\infty}\int O(u,v)\,e^{j(ux+vy)}\,du\,dv$$

giving

$$o(x,y) = \sum_{m=0}^{\infty}\sum_{n=0}^{\infty} a_n b_m \int_{\infty}^{\infty} \psi_k(u)\,e^{-jux}\,du \int_{\infty}^{\infty} \Phi_m(v)\,e^{-jvy}\,dv$$

where the integration is over the extrapolated spectrum due to the properties of the PSWF. Actually the inverse transform need not be taken because the PSWF are known to be their own space limited Fourier transforms when properly scaled. Therefore

$$\psi_n(u) = \frac{1}{2RA(j)^n} \int_{-A}^{A} e^{ju\xi} \psi_n\left(\xi \frac{\Omega}{2A}\right) d\xi$$

where R is a constant for a fixed space-bandwidth product $\left(C = \frac{A\Omega}{2}\right)$. For simplicity let $C = \frac{BW}{2}$. Then, the restored object

$$O(x,y) = \sum_{m=0}^{\infty} \sum_{n=0}^{\infty} a_n b_m \frac{(-j)^{n+m}}{4R^2AB} \psi_n\left(\frac{x\Omega}{2A}\right) \Phi_m\left(y\frac{w}{2B}\right)$$

$$\text{for} \quad \begin{cases} |X| \leq A \\ |Y| \geq B \end{cases}$$

is obtained without the need for the inverse Fourier transform.

The future direction at this stage is twofold. First, it should be noted that equation (4.3-1) for the orthogonal expansion holds with equality, in the mean square sense and individual components of the expansion can be large. In the computer the infinities of the equation must be accommodated to prevent arithmetic overflow. Secondly, the R, $\psi_n(u)$, and $\Phi_m(v)$ are all parametric in the space bandwidth product C. Therefore, updating the estimate of $\Phi(u,v)$ as one extrapolates (continues) into the diffraction limited area by parametrically adjusting R, $\psi_n(u)$, and $\Phi_m(v)$ becomes of considerable computational interest.

References

1. Harris, J. L., "Diffraction and Resolving Power," JOSA, Vol. 54, No. 7, pp. 931-936, (July 1964).

2. Frieden, B. R., "Band-Unlimited Reconstruction of Optical Objects and Spectra," JOSA, Vol. 57, No. 8, pp. 1013-1019 (August, 1967).

3. Harris, J. L., "Information Extraction from Diffraction Limited Imagery," Pattern Recognition, Vol. 2, No. 2, pp. 69-79 (May, 1970).

4. Slepian, D., and H. O. Pollak, "Prolete Spheroidal Wave Functions, Fourier Analysis and Uncertainty-I," BSTJ, Vol. 40, pp. 43-63 (January, 1961).

4.4 Generalized Wiener Filtering for Image Restoration

William K. Pratt

Wiener filtering is a classical technique of signal estimation that has been applied, primarily, to one dimensional, continuous signals, with analysis and implementation based upon continuous Fourier signal theory. It is possible, of course, to perform Wiener filtering operations on time sampled signals, and extend the technique to two dimensions. Furthermore, the filtering operation can be implemented by unitary transformations other than the Fourier transform. Finally, it is possible to significantly reduce the computational requirements without severely affecting performance by a technique of selective computation.

One Dimensional Filtering. Figure 4.4-1 is a block diagram of a generalized one dimensional Wiener filtering system. A zero mean, M element, data column vector, f, composed of additive, zero mean signal, s, and noise, n, components is the input to the system. The signal and noise are assumed uncorrelated with each other.

In the system a unitary transformation operation, utilizing an M by M transformation matrix, A, is performed on the input data vector yielding

$$F = Af = As + An \equiv S + N$$

Next, the transform input vector is multiplied by the M by M filter matrix, G. Note that, in general, G is not a diagonal matrix. If G contains off diagonal terms, the filtering operation, denoted as vector filtering, simply weights each spectral component of the input vector individually. In the final step an inverse unitary transform operation is performed to obtain the resultant estimate.

$$\hat{s} = A^{-1}GF = A^{-1}GAf$$

The filter matrix, G, is chosen in conjunction with the transformation matrix, A, so that the mean square error

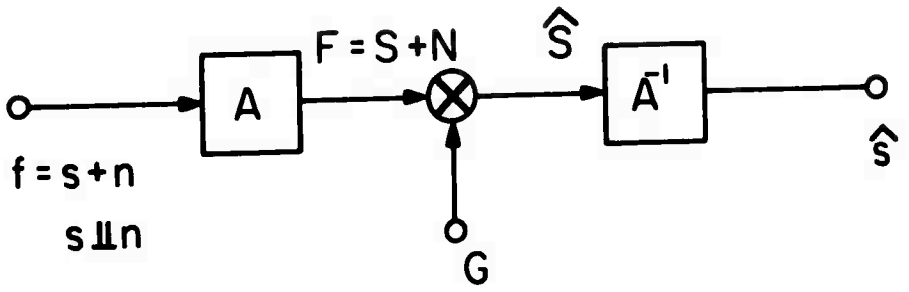

FIGURE 4.4-1 Generalized Wiener Filtering

$$e = Tr\left\{ \overline{(s-\hat{s})\,(s-\hat{s})^T} \right\}$$

Between the signal and its estimate is minimized.

Minimization of the m.s.e. by Lagrangian techniques yields the optimum filter matrix

$$G_o = C_S(C_S + C_N)^{-1}$$

where

$$C_S = A\,C_s\,A^{-1} \qquad C_N = A\,C_n\,A^{-1}$$

are the covariance matrices of the transformed signal and noise, respectively. The resulting minimum mean square error becomes

$$e_{min} = Tr\{C_S C_N (C_S + C_N)^{-1}\} = Tr\{C_s C_n (C_s + C_n)^{-1}\}$$

Note that the minimum m.s.e. is independent of the type of unitary transform employed. However, the character of the filter matrix, G, is dependent upon the unitary transform. The conclusion is that one is free to choose the transform that will minimize the computational processes entailed in filter generation and filter operation. A further savings in computational requirements can be obtained by a selective computation technique in which the smallest magnitude elements of the filter matrix are discarded. It has been found that for Fourier or Hadamard transform Wiener filtering up to 90% of the matrix multiplications can be eliminated with only a slight loss in optimum m.s.e. performance.

Two Dimensional Filtering. The Wiener filtering concept can be extended to two dimensions quite readily (details are presented in reference [2]). As a test of its validity, the concept of generalized Wiener filtering has been applied to the restoration of noisy images.

Figure 4.4-2a shows an original image containing a toy tank. The

(a) Original

(b) Original plus noise

Reproduced from best available copy.

(c) Optimal Hadamard Filtering

(d) Suboptimal Hadamard Filtering

Figure 4.4-2. Wiener Filtering Image Restoration Examples

image contains 256 by 256 elements and 64 grey scales. In Figure 4.4-2b uniformly distributed noise has been added to the original to produce an image with a signal-to-noise ration of unity. Figure 4.4-2c illustrates the effect of optimal Hadamard transform Wiener filtering in 16 by 16 blocks over the image surface. There is an obvious improvement in image quality, however, the grid pattern caused by the small block size is noticeable. The grid pattern in the filtered images can obviously be eliminated by filtering over the entire image, but at the expense of computational complexity. Alternatively, the grid pattern can be minimized by overlapping the filtering blocks or by spatial averaging at the interface between blocks. In Figure 4.4-2d the filtering operation was performed with 75% of the filter elements set to zero. The 25% of the filter elements retained are the largest magnitude elements of the filter matrix. Since the locations of the zero elements of the filtering matrix are known prior to the filtering operation, a computational algorithm can be employed to avoid multiplication by the zeros, and therefore, reduce the filtering computation requirements by the 75% factor. There is no apparent difference in the visual results for the optimal and suboptimal filtering examples.

References

1. W. K. Pratt, "Fast Computational Techniques for Generalized Two Dimensional Wiener Filtering," Proceedings Two Dimensional Digital Signal Processing Conference, October, 1971, pp. 1-1-1 to 1-1-10.

2. W. K. Pratt, "Generalized Wiener Filtering Computation Techniques," IEEE Transactions on Computers, July, 1972.

4.5 Color Image Restoration

Clanton-Mancill, William K. Pratt

It is the objective of any color imaging system to provide a spectral output at each image point which appears to the human observer to match the color of the corresponding point in the original scene. The colors reproduced by trichromatic systems such as color television, color

photography and color separation scanners generally exhibit color matching errors, such as shifts in hue and saturation. These errors are caused by spectrally imperfect sensor characteristics, system noise, and inherent system nonlinearities.

The study undertaken is concerned with the digital estimation of the color tristimulus values of light which exposes a color transparency film at a given image point. Observables for the estimation process are three color signals obtained from a flying spot scanner at the image point of the developed transparency. If the estimator is good, the image point color in the original scene can be colorimetrically matched by a television display or photographic record. This is true even if the image point spectial energy distribution of the illuminated transparency does not match the original image point spectial energy distribution.

A complete color separation and restoration system has been modeled in a digital computer program. A block diagram of the system under consideration is shown in Figure 4.5-1. A color transparency made from film of known sensitivity and dye characteristics is placed in a flying spot scanner. The three outputs of the filtered PMT detectors serve as the input to an estimation algorithm whose output is an estimate of the three layer exposures of the transparency at the image point. The exposure estimates $\hat{X}_R$, $\hat{X}_G$, $\hat{X}_B$ then become the input to a transformation algorithm which expresses the estimate as tristimulus values $\hat{U}, \hat{V}, \hat{W}$ of the original color which exposed the film. It is the purpose of the current study to optimize the algorithms for exposure estimation and tristimulus estimation. These algorithms could be incorporated into a digital processor which would provide fast, efficient and flexible color restoration.

Some results of work undertaken thus far are shown in Figure 4.5-2. Uniform chromaticity coordinates are plotted for ten input colors and for the corresponding computer simulated color representations of the scanner signals, the exposure estimates, and the tristimulus estimates.

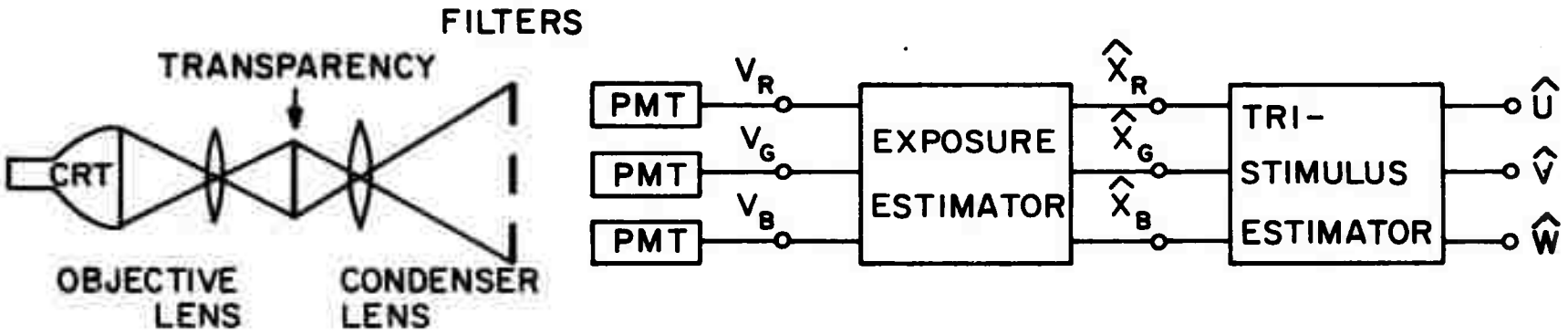

Figure 4.5-1 COLOR IMAGE TRISTIMULUS ESTIMATION SYSTEM

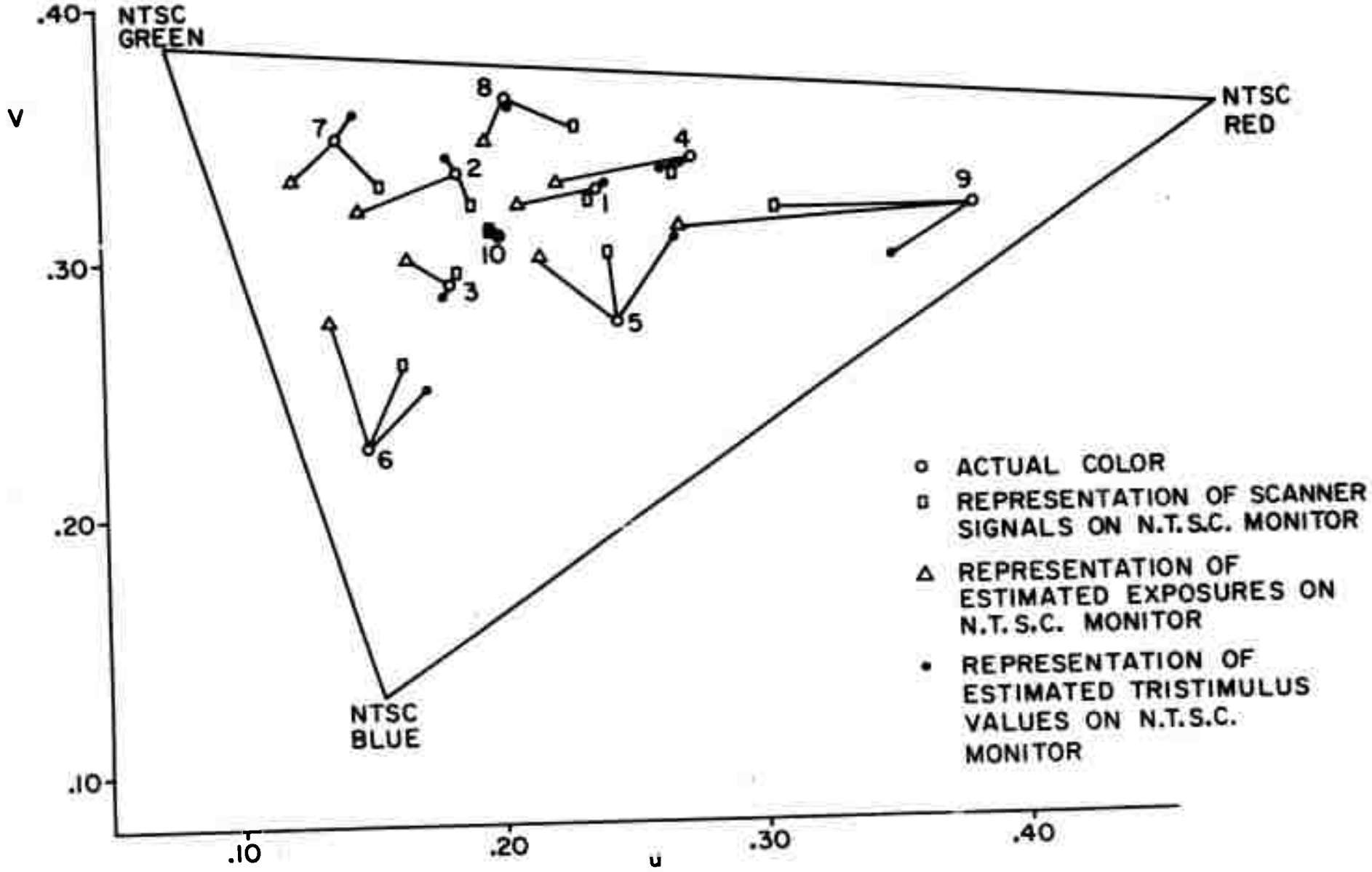

Figure 4.5-2 UCS chromaticity coordinates of test colors as represented by scanner signals, estimated exposures, and estimated tristimulus values.

The estimation of exposures from the scanner signals requires the simultaneous solution of three nonlinear integral equations. Solutions were obtained for the exposure estimates shown in Figure 4.5-2 by means of a Newton-Raphson iteration technique. Since exposure estimates are required at each picture element, a computationally simpler estimation algorithm is desirable. Work is now under way toward achieving a simple and accurate exposure estimator.

4.6 Pseudocolor Image Enhancement*

Andrews G. Tescher, Harry C. Andrews

There has been recent interest in the use of pseudocolor image transformations that map image grey scale into a sequence of colors in order to enhance the image quality or emphasize salient features of the image. An unconventional method of pseudocolor generation utilizing information theoretic principles is presented in the following sections [1].

Formulation. The following problem is typical in many image processing applications. A sampled intensity image of the form $I = I(j,k)$ $(j,k = 1,\ldots N)$ is given as the appropriate matrix of N^2 numbers. The object is to process I such that the improved image $I' = L(I)$, where L represents the entire processing, is more meaningful to the human viewer. The goal is to specify L such that the human visual information extraction process is improved by utilizing the appropriately processed image.

The samples represent intensity information in the original image; yet, the human eye is quite receptive to color as well as intensity changes. Therefore, the desired processing should allow for the decomposition of intensity into color. A color image, for most practical considerations, may be represented by three primary color components; consequently, the processing function L will include three separate transforms:

*Portions of this work were sponsored by the National Science Foundation (NSF-GK-20258).

L_{1x}, L_{1y}, and L_{1z} such that $X = L_{1x} I$, $Y = L_{1y} I$, and $Z = L_{1n} I$. The variables X, Y, and Z are matrices of N^2 points. In order to utilize the entropy approach, one considers X, Y, and Z as sample functions of a random process with a probability density function P(X, Y, Z). The associated entropy is defined as

$$H(X, Y, Z) = \sum_X \sum_Y \sum_Z P(X, Y, Z) \log P(X, Y, Z)$$

where the summation is over all quantum levels in the component images. As the first step to maximize H, the entropy associated with the individual images is maximized. It can be shown that for any of the component images (e.g., X), H(X) is maximal when all values of X are equally likely. Therefore, the component images must be transformed such that $X' = L_{2x} X$, $Y' = L_{2y} Y$, $Z' = L_{2z} Z$, and $P(X') = P(Y') = P(Z') = 1/M$, where each image is assumed to be digitized to M quantum levels.

It is well known that H(X, Y, Z) is maximal whenever P(X), P(Y), and P(Z) are independent. Consequently, another set of transforms is required such that for L_{3x}, L_{3y}, and L_{3z} and for $X'' = L_{3x}(X', Y', Z')$, $Y'' = L_{3y}(X', Y', Z')$, and $Z'' = L_{3z}(X', Y', Z')$; $P(X'', Y'', Z'') = P(X'')P(Y'')P(Z'')$ is obtained. Consequently, for the image sets X", Y", and Z", the inequality $H(X'', Y'', Z'') \geq H(X, Y, Z)$ must be satisfied.

Experimental Implementation. An intensity image sampled at 256 x 256 rectangular grid locations was chosen to demonstrate the principle discussed above. The L_1 transforms were specified as the rotationally symmetric low-pass, band-pass, and high-pass filters for L_{1x}, L_{1y}, and L_{1z}, respectively. Thus, the frequency plane is separated by the concentric circles of radii 0.1 and 0.25 into three nonoverlapping regions.

The L_2 transforms are the individual distribution functions for the three component images; for example, an arbitrary element in the X'

image is written as follows:

$$X'(i,k) = F(X(i,k))$$

where $F(S) = \int_{-\infty}^{S} P(X)\, dX$.

If Gaussian statistics are assumed, the L_3 transforms are the rotation matrices composed of eigenvectors of the 3 x 3 covariance matrix for the X', Y', and Z' images. Rotation matrices both with and without the application of the L_2 transforms are listed below.

$$\begin{bmatrix} 0.000 & 1.000 & 0.006 \\ 0.949 & -0.002 & 0.315 \\ -0.315 & -0.005 & 0.949 \end{bmatrix}$$

(a) With the L_2 transform

$$\begin{bmatrix} 0.346 & 0.886 & 0.311 \\ 0.706 & -0.464 & 0.535 \\ -0.618 & -0.035 & 0.786 \end{bmatrix}$$

(b) Without the L_2 transform

Calculated Covariance Matrices

In the latter case, the mixing of component images becomes considerably emphasized. Figure 4.6-1 illustrates the same point. Images a, b and c are the X", Y", Z" images without the L_2 transforms; they remain essentially the band-pass filtered images. For images a, b, and c of Figure 4.6-2 the same procedure is repeated with the L_2 transforms; the effect is strong mixing of the component images.

Considerably more research remains to be done in selecting and

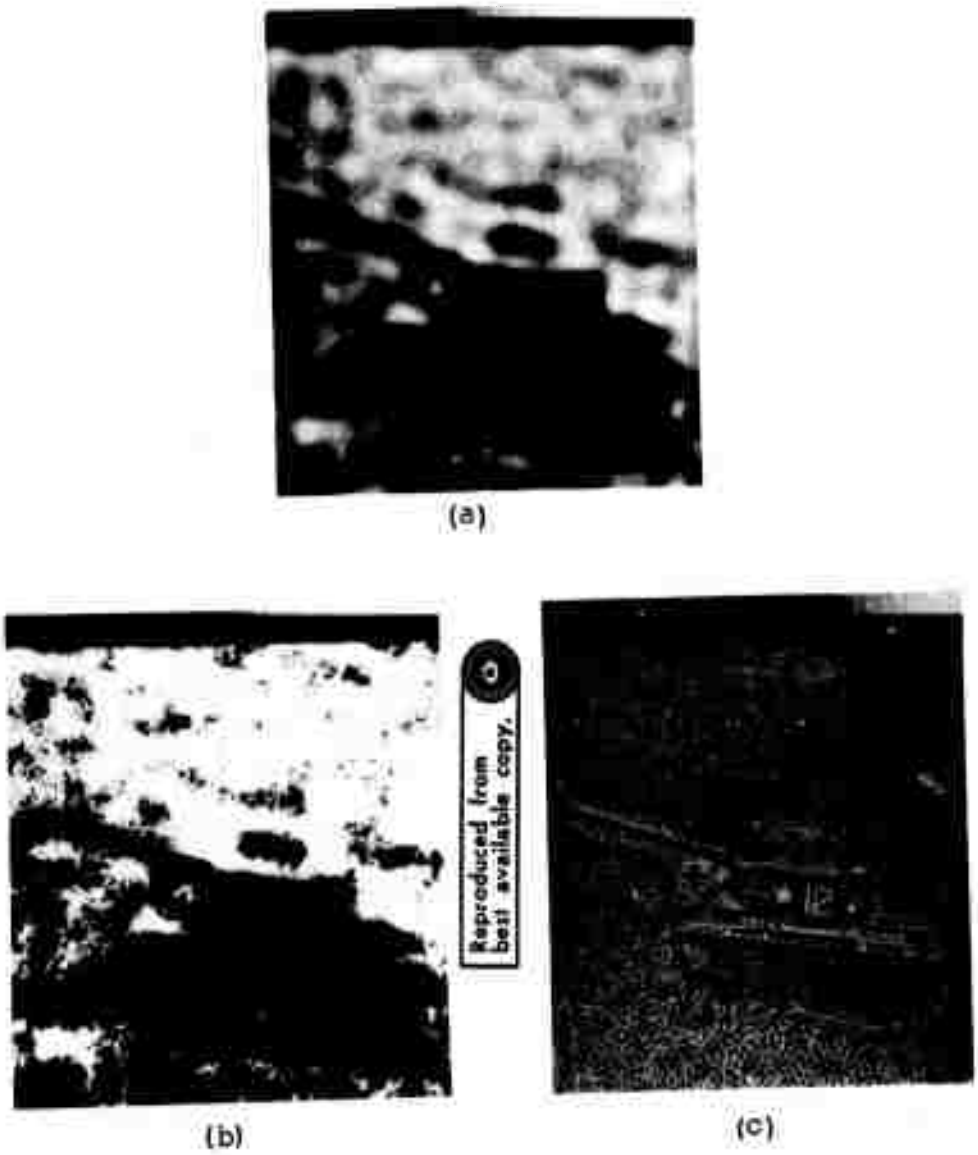

Reproduced from best available copy.

Figure 4.6-1. Image decomposition into primary components without the L_2 transforms.

(a)

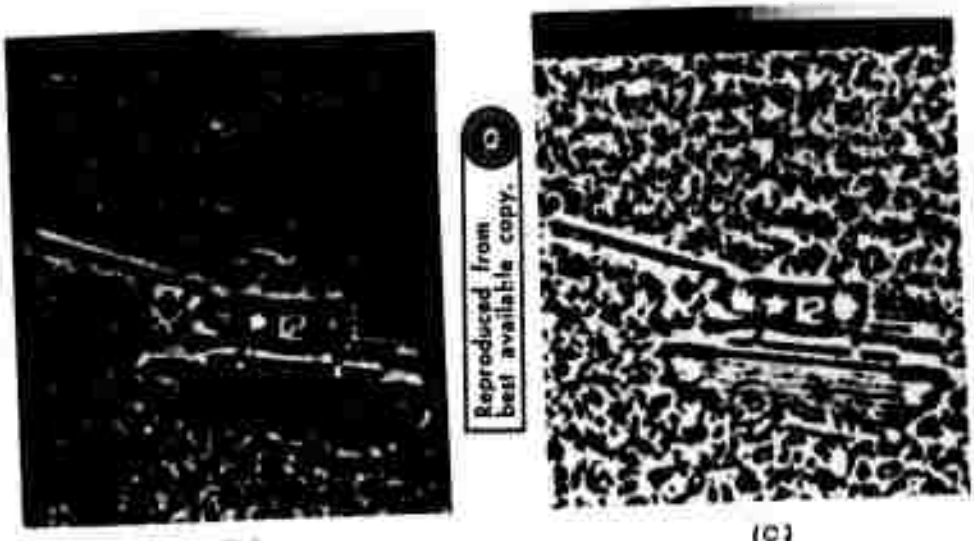

(b) (c)

Figure 4.6-2. Image decomposition into primary components with the L_2 transforms.

optimizing various transform candidates. The generalized techniques of pseudo color transformations may result in powerful image enhancement procedures.

Reference

1. A. G. Tescher and H. C. Andrews, "Image Display Enhancement and Maximum Entropy," 5th Annual Hawaii International Conference on Systems, January, 1972.

4.7 Nonlinear, Heuristic, and Positive Restoration Image Enhancement Processes*

Harry C. Andrews

Nonlinear Processes. Some of the most exciting results in digital image enhancement lie in the area of nonlinear processing. Certain aberrations (coma) and camera motion blur can be corrected with known nonlinear techniques. However, two such techniques which have been investigated recently lie in the use of the Fourier or Walsh transform of an image (a linear process) followed by a nonlinear operator followed by the inverse linear process. If an image is defined by the function $f(x, y)$ and its Fourier, Walsh, or Unitary transform, in two dimensions, is defined by $F(u, v)$ then two nonlinear operations of interest are $\log |F(u, v)|$ and $|F(u, v)|^{\alpha}$ where the magnitude of the transform coefficients are nonlinearly modified. In the logarithmic technique a generalized cepstrum processor results and in the α power technique, for $\alpha < 1$ a generalized rooting occurs. Both approaches have the effect of reducing the large magnitude components in favor of the smaller components, thus, assigning (nonlinearly) more weight to those frequencies (or coefficients) which are less obvious in the original image. Results in this area of research are quite pleasing visually (see Figure 4.7.1).

*Portions of this research were sponsored by the National Science Foundation (NSF-GK-20258).

(a) $\alpha = 1$ Original

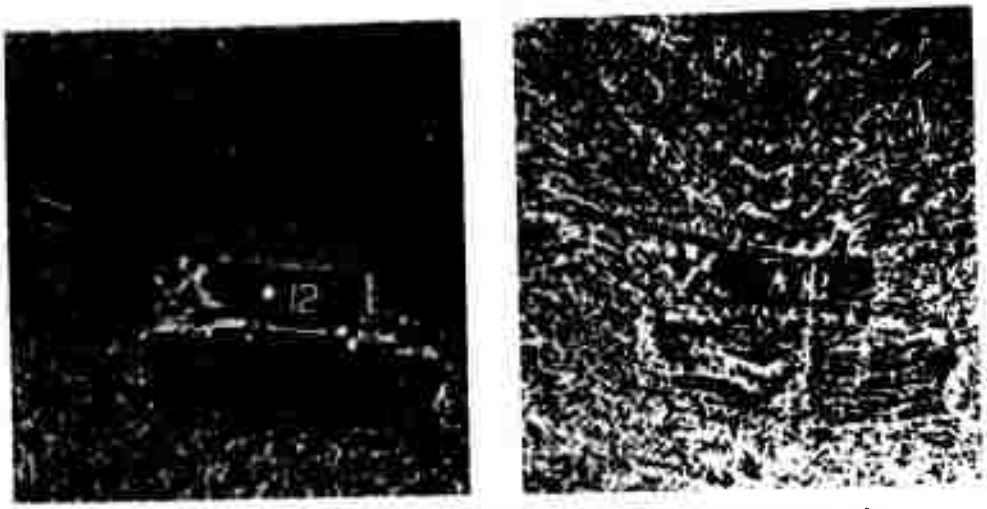

(b) $\alpha = 1/2$ Square root of Fourier magnitude

(c) $\alpha = 0$ Phase information only

Reproduced from best available copy.

Figure 4.7-1. Example of α Rooting for Image Enhancement

Heuristic Spatial Techniques. There are a variety of heuristic techniques, all of them nonlinear, which provide for digital image enhancement without the use of orthogonal transform spaces. Some of the simplest of these might be the stretching or shrinking of gray scale information in order that certain regions of brithness become more evident. Another trivial technique for computer implementation is bit removal in which it becomes possible to determine features of an image by independently investigating various bit planes of data. This is particularly useful for investigating geometric shapes in shadow regions of a photograph. Finally, one heuristic spatial domain technique which is finding wide and exciting use in digital image enhancement is known as histogram equalization. In this approach a histogram (experimentally determined probability density function) is formed from an image. The image is then requantized to force the histogram to be as uniform as possible, thereby, maximizing the zero memory entropy of the image. The technique has the effect of redistributing shades of gray such that sublties in dominant shades of gray become more obvious while slight changes in less dominant gray areas become less noticeable. Results in x-ray digital image enhancement have successfully used the technique. Theoretical investigations in these areas are underway.

Positive Restoration. The subject of positive restoration implies that the a priori knowledge that both the image and object are positive quantities (intensities) plays a dominant role in the restoration technique. Often this property is ignored but in fact its relevance to the restoration technique is quite critical. Previous work in this area has been limited to one dimensional functions (images) such as spectrometer outputs and other instruments which are inherently intensity measuring devices [1-3]. Two of the approaches tend to be iterative in nature both converging to a highly resolved spectra which provides considerable improvement than the original image [1-2]. The third technique utilizes a maximum likelihood approach in which close analogy with the derivation of Maxwell-Boltzmann

statistics is maintained [3]. In this technique, the image is guaranteed to be positive according to an exponentiation resulting from the maximum-likelihood estimate. Again for one dimensional positive images, results are quite encouraging. Other methods requiring both one and two dimensional implementation include modeling the image as a joint probability density function, as a two dimensional power spectrum and as the result of multiple positive convolutions. It is anticipated that extension of these and other techniques associated with positive restoration on large scale digital computers to two dimensional images will have rewarding consequences.

References

1. Biraud, Y., "A New Approach for Increasing the Resolving Power by Data Processing," Astron. and Astrophys., Vol. 1, pp. 124-127 (1969).

2. Jansson, P. A., R. H. Hunt, and E. K. Plyler, "Resolution Enhancement of Spectra," JOSA, Vol. 60, No. 5, pp. 596-599 (May 1970).

3. Frieden, B. R., "Restoring with Maximum Likelihood," Optical Sciences Center, University of Arizona, Technical Report No. 67 (February 1971).

5. Image Support Projects

The following sections describe the research facilities of the Image Processing Group, an image processing software system developed at the University Computer Center, and the publication of a bibliography on digital image processing.

5.1 Image Processing Research Facilities

Figure 5.1-1 contains a block diagram of the U.S.C. image processing facilities. For digital image processing operations the user has available several interconnected computers with a variety of hardware and software configurations. The University Computer Center's (UCC) IBM 370/155 is used for large scale, computation bound problems. Image processing programs at UCC are run under the VICAR image processing language. Smaller scale image processing problems are run on the IBM 360/44 in the Engineering Computer Laboratory. The 360/44 acts as the host computer for connection to the ARPA computer net via the TIP interface unit. The TIP and associated communications equipment are scheduled for installation by 1 April 1972. The Image Processing Laboratory contains two mini-computer systems: a Hewlett-Packard 2100 for command and control of image acquisition and display devices and an Interdata IV for real time simulation of image processing systems. With the HP-2100 it is possible to interact in real time with the image processing devices and with the larger computers in the facility.

Figure 5.1-2 contains photographs of some of the equipment in the Image Processing Laboratory. Capabilities of the image processing acquisition and display devices are listed below:

Flying Spot Scanner

Utilization:	digitization of monochrome and color transparencies and recording of monochrome and color images on Polaroid and 35 mm film

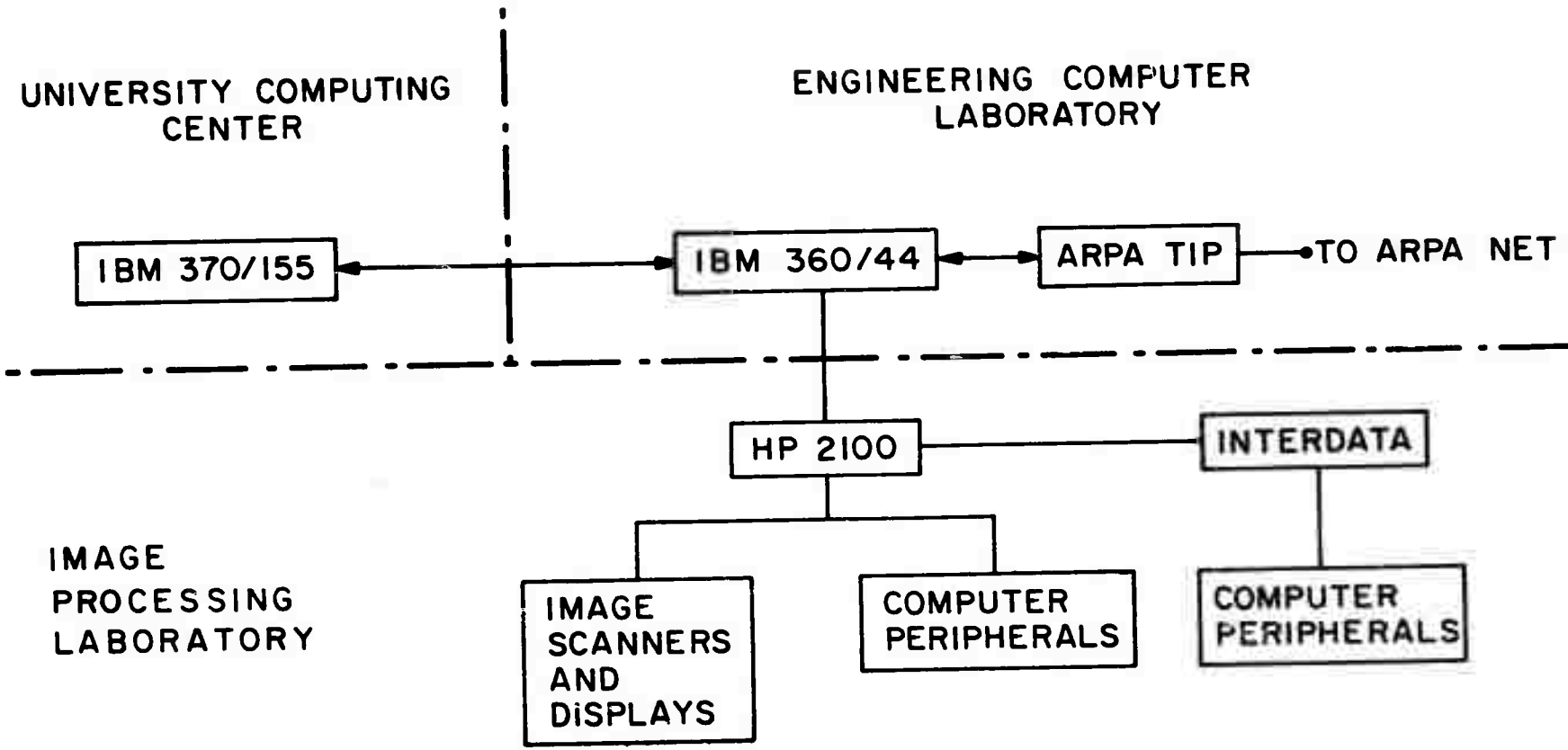

Figure 5.1-1. USC IMAGE PROCESSING LABORATORY FACILITIES

Spatial resolution:	1024 by 1024 pixels
Diplay grey scales:	256 quantization levels computer compensated for CRT and film nonlinearities
Digitization grey scales:	256 linear quantization levels of transparency transmittance
Scan time:	1 to 10 sec.
Phosphor:	LP203, "white" spectrum for color work
Image:	0.75" by 0.75" or 2.25" by 2.25"

Color Facsimile Unit

Utilization:	digitization and recording of monochrome and color prints
Spatial resolution:	100 lines/inch
Grey scales:	64 quantization levels each for red, green, and blue signals
Scan time:	12 min.
Image size:	8" by 10"

Real Time Display

Utilization:	real time display of monochrome and color digital images
Spatial resolution:	576 horizontal and 525 vertical lines on shadow mask CRT
Grey scale:	64 quantization levels each for red, green, and blue signals
Write time:	10 sec.
Refresh rate:	60 fields/sec.
Storage medium:	digital disk

HP 2100A and peripherals

Interdata and peripherals

HP 2116B and peripherals

Figure 5.1-2. Image Processing Laboratory Equipment

All of the above units are connected to the HP-2100 computer and are directly accessible to the ARPA computer network.

5.2 Image Processing Capabilities at the USC University Computing Center

Richard P. Kruger

The software configuration at the University Computing Center (UCC) consists of two distinct but interacting software systems. For want of a better title, they will be referred to as the VICAR and NON-VICAR systems.

The VICAR (Video Image Communication and Retrieval) system was developed by a co-operative effort of the Jet Propulsion Laboratory and IBM in 1968 and a current OS version has been operational at UCC since November 1971. The purpose of VICAR is to facilitate the acquisition, digital processing and recording of image data. System objectives include ease of operation for scientific personnel not familiar with systems programming knowledge as well as the capability to perform digital image processing on a production basis.

VICAR usage can be divided into the three categories of system, application, and problem programming. The system programmer requires knowledge of application and problem programming only in a global sense. The application programmer is capable only of using existing problem programs and requires no knowledge of either system or problem programming. The problem programmer must of course have knowledge of application program protocol but need have system programming capabilities.

From a system viewpoint, the operation of the VICAR system is very similar to that of a standard utility program. The application programmer provides a card deck containing the job in the form of VICAR control statements which define the processing tasks. VTRAN, the VICAR

compiler, uses these statements to generate any required OS-JCL as well as a job task queue JCFILE. Then VTRAN returns control to OS. Next a system program VMAST (VICAR master) is loaded and remains in core throughout the job to supervise the JCFILE processing up to fourteen (14) simultaneous I/O requests with random or sequential direct disk data set or tape access. VMAST handles the task queue through a system program JCFILE which is called into core by VMAST for each job task. This procedure is shown in Figure 5.2-1.

Standard tape formats have been established for both tape and disk data sets. Table 1 is a list of VICAR compatible tape formats.

	FORMAT CODE	TAPE LABEL
1.	9 nine track 800 bpi, 8 bit/pixel	standard
2.	8 seven track 800 bpi, 8 bit/pixel	standard
3.	5 seven track 556 bpi, 6 bit/pixel	standard
4.	9A nine track 800 bpi, 8 bit/pixel	no label
5.	8A seven track 800 bpi, 8 bit/pixel	no label
6.	8F seven track 800 bpi, 6 bit/pixel	no label
7.	5F seven track 556 bpi, 6 bit/pixel	no label
8.	2F seven track 200 bpi, 6 bit/pixel	no label

Table 1. VICAR compatible tape and disk formats

Each tape label is 360 bytes long and is divided into five 72 byte blocks. The first block consists of system information such as number of lines (NL) and (NS) in the input and output images. Subsequent 72 byte blocks consist of system or user added history or information labels. System and user labels precede the image data. Such labels are useful in preserving the processing history of a particular image.

A second level of VICAR usage is that of application programming. It only requires knowledge of a finite number of control statements all of

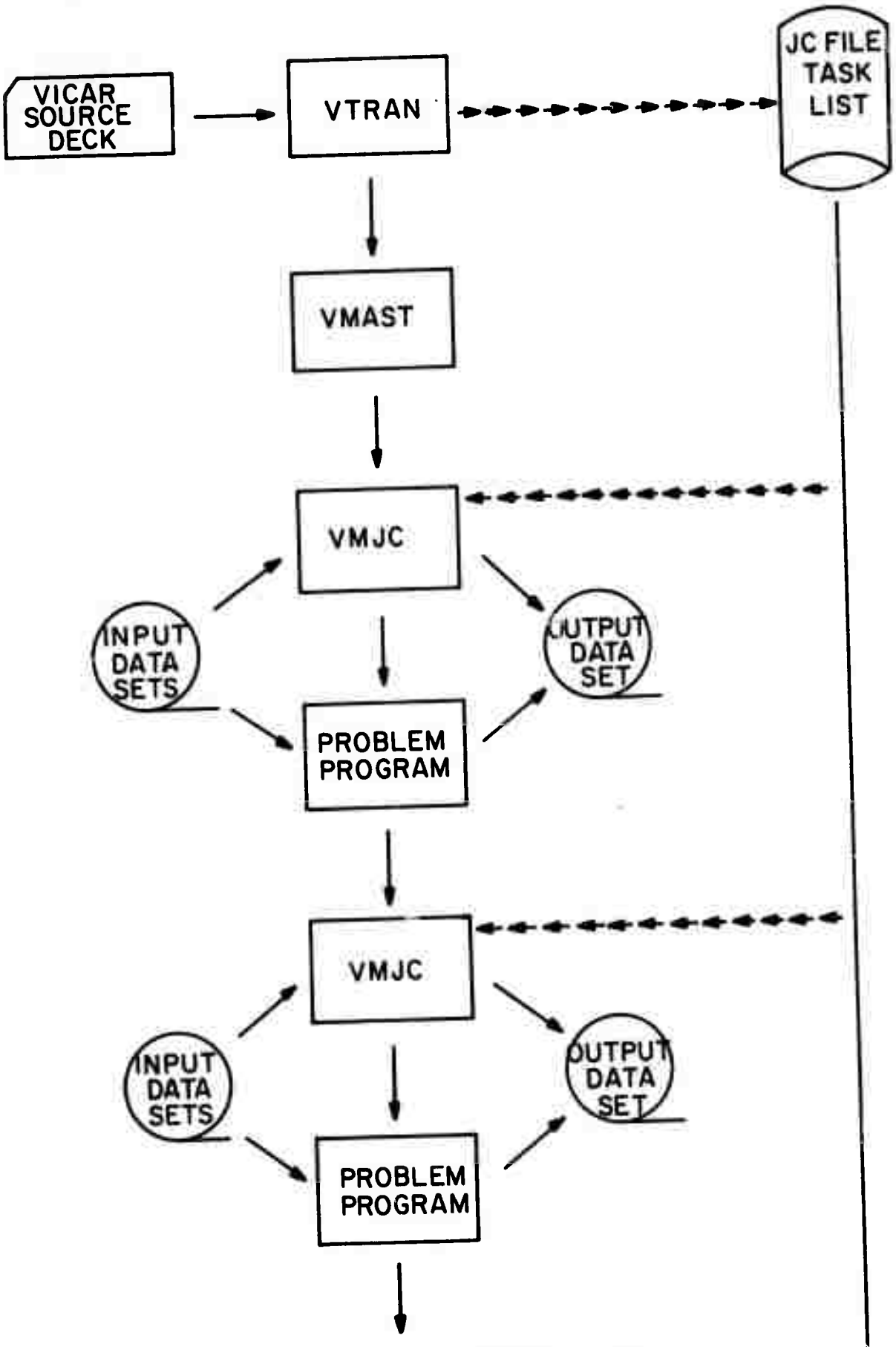

Figure 5.2-1 – VICAR SYSTEM LOGIC

which exhibit a standard format. These statements are listed in Table 2.

CONTROL STATEMENT	DESCRIPTION OF PURPOSE
RESERVE	reserve direct access disk data sets
SAVE	save a data set in job 1 for a subsequent job
FIND	access data sets created in a previous job
READ	define device and data format for an input tape
WRITE TAPE	define device and data format for an output tape
EXEC	define task (problem program) I/O and parameters
PARAMS	define a symbolic name to pass parameters to the calling program
LABEL RELABEL	specify user label to label block of output image
DEBUG	generates FTO6JCL statement making Fortran I/O possible
END	indicates the last control statement

Table 2

Each EXEC statement calls a problem program from VICARLIB to perform a desired task. The calling format is standard with respect to all problem programs. Figure 5.2-2 is an example of a VICAR application program.

Briefly described, this application program reads a 500 by 500 pixel into the program, reverses it about its vertical axis, geometrically reduces it to 256 by 256 pixels, and adds various grid line markings. These processed images are then written sequentially on tape for later displays. In addition, the four processed images are concentrated into one disk data set and written onto a second tape. Some of these results are shown in Figure 5.2-3.

```
KEFV0123 STEP1

ACCT,(EFV01AR,RK)
NAME,KRUGER
REGION,320K
TIME,0005
READ,TAPE9,001791,TX
TAPE,TAPE8,(ASK002,D3,D4,D5),TB
WRITE,TAPE7,(PHD001,D8),TC,SF
RESERVE,4,260,260,2314,(D2,D3,D4,D5)
RESERVE,2,600,600,2314,(D1,D6)
RESERVE,2,1100,1100,2314,(D7,D8)
E,LIST,*TB02,*,(1,1,1,1),(PRINT,NOHIST)
E,FLOT,*TX01,D1,,HORIZONTAL
E,GEOM,D1,D2,(1,1,256,256),G2
PARAMS,G2
SAMPLE          1          256
LINE      1     0,0        244,0
LINE      256   0,244      244,244
E,GRID,D2,D3,,
E,MAPGRID,D2,D4,,BLACKWHITE
E,MAPGRID,D2,D5,,(MODULATE,64)
E,CONCAT,(D2,D3,D4,D5),D6,(1,1,512,512)
E,VGEN,*,D7,(1,1,1024,1024),(0,0,0)
E,INSECT,(D7,D6),D8,(1,1,1024,1024),P
PARAMS,P
        1          1          512  512  256  256
END

 13 TASKS FOR THIS STEP
```

Figure 5.2-2. Example of VICAR application program

(a) Output of GRID

(b) Output of MAPGRID

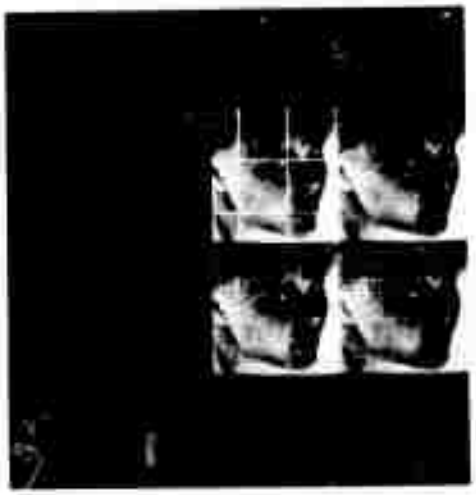

(c) Output of CONCAT

Reproduced from best available copy.

(d) Original image

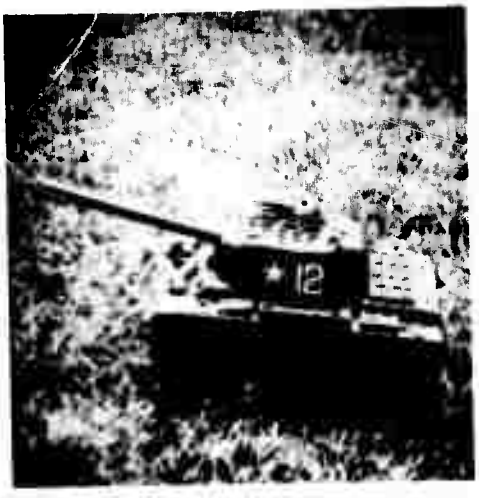

Image processed by Gaussian isotropic high frequency emphasis filter followed by histogram equalization

Figure 5.2-3. Examples of images processed by VICAR.

A third level of VICAR knowledge is that of the problem programmer. At this level the individual has knowledge of both application and problem programming protocol, but requires little system programming knowledge. The problem programmer can add to the problem program library as well as use existing software. The problem program can be written either in Fortran or Assembly language and differs from a normal subroutine only in its I/O structure. In addition to normal Fortran I/O, VICAR I/O statements must be included. These are included in Table 3 and are stored as subroutines in VICARSUB.

STATEMENT CALL	DESCRIPTION OF USAGE
OPEN	open data set and defines its buffering for the task
PARAM	reads system and user parameters into problem program
READ	reads record onto input data set
WRITE	writes record onto output data set
CHECKR	checks status of last I/O request
PRINT	prints typewritten and/or printer on-line messages
END	normal end
ABEND	abnormal termination of problem program

Table 3

Most existing Fortran subroutines can easily be converted into VICAR application programs. Figure 5.2-4 shows a portion of a Fortran subroutine with added VICAR I/O appearing as the un-numbered cards.

At present VICAR contains approximately 30 application programs. These programs perform such varied functions as Fourier transformations, picture annotation, line plotting, and filtering.

NON-VICAR image processing at UCC is considerably less flexible and more restrictive. I/O is presently limited to 256 by 256 pixel images. However, approximately 60 conventional Fortran and Assembly language programs are available for call on IPLLIB. These subroutines perform such diverse functions as image scaling, linear and non-linear filtering, histogramming and pictorial pattern recognition.

Job control statements are necessary to properly use this sytem but because of its relative simplicity these are of a standard format. Figure 5.2-3 shows an example of image processing from this library.

The NON-VICAR processing is useful for more experimental processing where VICAR sophistication, flexibility, and production capabilities are not necessary. It should also be noted that I/O formats for both systems are compatible and each in turn is compatible with the Image Processing Library.

5.3 Image Processing Bibliography

A bibliography entitled: "Bibliography on Digital Image Processing and Related Topics", has been published as USCEE Report 410. The bibliography is an attempt to gather together references to the vast amount of pertinent literature in the field of digital image processing. It is arranged into three sections: classification by subject; classification by last name of first author, classification by year of publication. A listing of the subject classifications is on the following page. The bibliography has been stored on punched cards and magnetic tape for ease of editing and updating. Plans are to issue periodic editions of the bibliography so that new and previously overlooked works may be included. The following page references Section A of the Bibliography: Classification by subject.

```
LEVEL  19                    LNEPLT              DATE = 72054          17/26/52

      SUBROUTINE LNEPLT
       INTEGER SLO,SSO,ODS,FSI,FSI1
      INTEGER PAR(32),IBUFA(300),OBUFA(300)
      INTEGER*2 IBUF(1200),OBUF(1200)
      DIMENSION A(1100,9)
      DIMENSION NYAXIS(1,101),SYMBOL(9),YAXS(101)
      INTEGER MINUS,PLUS,YAXIS,XAXIS,BLANK,DOT,ASK,SYMBOL,ERROR,COUNT                 3
      INTEGER FMT(26),COMMA,A1,BLANKS,STORE( 101),TFIELD,RELOAD(3)                    4
      INTEGER PLOT,EXPONT(101)                                                        5
      REAL LOWERB                                                                     6
      LOGICAL NCHECK(101)                                                             7
      DATA STORE/      4HT018,4HT019,4HT020,4HT021,4HT022,4HT023,                     8
     14HT024,4HT025,4HT026,4HT027,4HT028,4HT029,4HT030,4HT031,4HT032,                 9
     24HT033,4HT034,4HT035,4HT036,4HT037,4HT038,4HT039,4HT040,4HT041,                10
     34HT042,4HT043,4HT044,4HT045,4HT046,4HT047,4HT048,4HT049,4HT050,                11
     44HT051,4HT052,4HT053,4HT054,4HT055,4HT056,4HT057,4HT058,4HT059,                12
     54HT060,4HT061,4HT062,4HT063,4HT064,4HT065,4HT066,4HT067,4HT068,                13
     64HT069,4HT070,4HT071,4HT072,4HT073,4HT074,4HT075,4HT076,4HT077,                14
     74HT078,4HT079,4HT080,4HT081,4HT082,4HT083,4HT084,4HT085,4HT086,                15
     84HT087,4HT088,4HT089,4HT090,4HT091,4HT092,4HT093,4HT094,4HT095,                16
     94HT096,4HT097,4HT098,4HT099,4HT100,4HT101,4HT102,4HT103,4HT104,                17
     44HT105,4HT106,4HT107,4HT108,4HT109,4HT110,4HT111,4HT112,4HT113,                18
     44HT114,4HT115,4HT116,4HT117,4HT118 /                                           19
     .DATA FMT/4H(T7,,4H1PE1,4H1.4,,4H    1,4H01(1,4HHY),,4H1HX,,4H      ,          20
     14H     ,4H     ,4H     ,4H     ,4H     ,4H     ,4H     ,4H     ,4H     ,     21
     24H     ,4H     ,4H     ,4H     ,4H     ,4H     ,4H     ,4H     ,4H     /     22
      DATA A1,LASTA1,BLANKS /4H,A1,,4H,A1),4H     /                                  23
      DATA RELOAD / 4H    1,4H01(1,4HHY), /                                          24
      DATA MINUS,PLUS,XAXIS,YAXIS,BLANK,DOT,ASK/ 1H-,1H+,1HX,1HY,1H ,                25
     1 1H.,1H* /                                                                     26
      DATA A/9900*0./
      EQUIVALENCE(SLO,PAR(1)),(SSO,PAR(2)),(NLL,PAR(3)),(NSO,PAR(4)),
     1(NLI,PAR(5)),(NSI,PAR(6)),(IDS,PAR(7)),(ODS,PAR(8)),(NA,PAR(10)),
     2(M,PAR(11)),(NL,PAR(12)),(NSTART,PAR(13)),(NEND,PAR(14)),
     3(FSI,PAR(15)),(LSI,PAR(16)),(LST1,PAR(17)),
     4(NOL1,PAR(18)), (LST2,PAR(19)),(NOL2,PAR(20)),(LST3,PAR(21)),
     5(NOL3,PAR(22)),(LST4,PAR(23)),(NOL4,PAR(24)),(LST5,PAR(25)),
     6(NOL5,PAR(26)),(LST6,PAR(27)),(NOL6,PAR(28)),(LST7,PAR(29)),
     7(NOL7,PAR(30)),(LST8,PAR(31)),(NOL8,PAR(32))
      CALL PARAM(INO,PAR,NA)
      WRITE(6,6000) NEND,NSTART,NA
 6000 FORMAT(3I7)
      CALL CHECKR(IND,&1440)
      CALL OPEN(NLR,2,0,0,IBUFA,1200)
      IF(NLR.LT.1) CALL ABEND
      NINT=NEND-NSTART+1
      DO 3330 I=1,NINT
 3330 A(I,1)=NSTART+I-1
      DO 3332 I=2,M
      GO TO (3333,3333,3334,3335,3336,3337,3338,3339,3329),I
 3333 LINEI=NLR+LST1
      NLO=NOL1
      GO TO 3340
 3334 LINEI=NLR+LST2
```

Figure 5.2-4. Example of VICAR subroutine

```
LEVEL  19                    LINEPLT                DATE = 72054          17/26/52

      NLO=NOL2
      GO TO 3340
 3335 LINEI=NLR+LST3
      NLO=NOL3
      GO TO 3340
 3336 LINEI=NLR+LST4
      NLO=NOL4
      GO TO 3340
 3337 LINEI=NLR+LST5
      NLO=NOL5
      GO TO 3340
 3338 LINEI=NLR+LST6
      NLO=NOL6
      GO TO 3340
 3339 LINEI=NLR+LST7
      NLO=NOL7
      GO TO 3340
 3329 LINEI=NLR+LST8
      NLO=NOL8
 3340 CONTINUE
      FSI1=FSI-1
      NP=LSI-FSI+1
      DO 3342 J=1,NLO
      CALL READ(IN1,2,LINEI,1,FSI1,NP,IBUF,0)
      CALL CHECKR(IN1,&1550)
      DO 3341 K=1,NP
 3341 A(K,I)=IBUF(K)+A(K,I)
      LINEI=LINEI+1
 3342 CONTINUE
      DO 3332 J=1,NLO
 3332 A(K,I)=A(K,I)/FLOAT(NLO)
      CALL OPEN(IN3,1,1,0,OBUFA,1200)
      NSO2=NSO*2
      DO 4000 I=2,NLL
      DO 4001 J=1,NSO
 4001 OBUF(J)=A(J,I)
      CALL WRITE(IN4,1,0,1,0,NSO2,OBUF,0)
      CALL CHECKR(IN4,&1660)
 4000 CONTINUE
      CALL CLOSE(IND,2,1)
      CALL CLOSE(IND,1,1)                                                    63
      SYMBOL(1) = DOT                                                        64
      SYMBOL(2) = ASK                                                        65
      SYMBOL(3) = PLUS                                                       66
      SYMBOL(4) = XAXIS                                                      67
      WRITE(6,5)                                                             68
    5 FORMAT( 1H1 )                                                          69
      COUNT = 0                                                              70
      ERROR = 0                                                              73
      NVAR = M - 1                                                           74
C     LOADING OF ALPHAMERIC FIELDS INTO OBJECT TIME FORMAT FMT               75
      J = 7 + NVAR*2                                                         76
      DO 15 JRC = 9,J,2                                                      77
      FMT(JRC) = A1
```

Figure 5.2-4. Example of VICAR subroutine (continued)

IMAGE ANALYSIS
Psychological properties of images
Image structure
Image quality measures
Statistical and information theoretic properties of images
Source and channel noise effects on images
Unclassified image analysis

IMAGE CODING AND TRANSMISSION
One dimensional data compression techniques with potential application to image coding
Basic pulse code modulation, quantization reduction coding, run length coding, and related image coding techniques
Differential pulse code modulation, predictive and interpolative coding, delta modulation, and related image coding techniques
Transform coding of images
Television frame-to-frame coding
Color image coding
Image coding reviews
Unclassified image coding

IMAGE ENHANCEMENT AND RESTORATION
Image restoration
Image enhancement
Pseudocolor and false color
Unclassified image enhancement and restoration

IMAGE DETECTION
Image detection techniques
Pattern recognition applied to image processing
Unclassified image detection

MISCELLANEOUS
Image processing computer languages
Image processing equipment
Image processing computational techniques
Image processing linguistics
Holographic, optical, and electro-optical techniques applied to image processing
Biomedical image processing
Image processing books and bibliographies
General image processing techniques
Unclassified image processing

6. Publications

The following is a list of papers, articles, nd reports published or accepted for publication during the past six months, that have resulted from ARPA sponsored research.

A. Habibi, "Two-Dimensional Bayesian Estimate of Images," Proceedings IEEE, Vol. 60, No. 7, July 1972.

A. Habibi, "Coding Color Images by Differential Pulse Code Modulation," Proceedings International Telemetering Conference, October 10-12, 1972.

N. E. Nahi and T. Assefi, "Bayesian Recursive Image Enhancement," Proceedings Two Dimensional Image Processing Conference, University of Missouri, October, 1971; and IEEE Transactions on Computers, July, 1972.

N. E. Nahi, "Role of Recursive Estimation in Statistical Image Enhancement," Proceedings IEEE, July, 1972.

J. Pearl, H. C. Andrews, and W. K. Pratt, "Performance Measures for Transform Data Coding," IEEE Transactions on Communication Technology, June, 1972.

William K. Pratt, "Generalized Wiener Filtering Computation Techniques," IEEE Transactions on Computers, July, 1972.

William K. Pratt, "Binary Symmetric Channel Effects on PCM Color Image Transmission," IEEE Transactions on Information Theory, (to be published, 1972).

William K. Pratt, "Walsh Functions in Image Processing and Two Dimensional Filrering," Symposium on Applications of Walsh Functions, March, 1972.

William K. Pratt, Lloyd R. Welch, and Wen-Hsiung Chen, "Slant Transforms for Image Coding," Symposium on Applications of Walsh Functions, March, 1972.

A. A. Sawchuk, "Linear Space-Variant Motion Degradation and Restoration," Spring Meeting of the Optical Society of America, New York, April 1972.

A. A. Sawchuk, "Space-Variant Image Motion Degradation and Restoration," Proceedings IEEE, Vol. 60, No. 7, July, 1972.

C. Reader, Spatial Subsampling for the Transform Coding of Images," Symposium on Applications of Walsh Functions, Washington, D. C., March 1972.